Organic & Biomolecular Chemistry

ROYAL SOCIETY OF CHEMISTRY

PAPER

View Article Online
View Journal | View Issue

Check for updates

Cite this: *Org. Biomol. Chem.*, 2025, **23**, 7298

Iodine-promoted oxidative cross-coupling for the synthesis of (*E*)-2-(3-oxo-3-phenylprop-1-en-1-yl)-3-phenylquinazolin-4(3*H*)-one *via* C–H activation: development of synthetic TLX agonists†

Lingaiah Maram,[a,b,c] Puhan Zhao,[a,b,c] Thomas Koelblen,[d,e] Lamees Hegazy,[b,c] Thomas P. Burris[d,e] and Bahaa Elgendy *[a,b,c]

Received 24th April 2025,
Accepted 10th July 2025

DOI: 10.1039/d5ob00672d

rsc.li/obc

We report the development of an efficient iodine-promoted oxidative cross-coupling reaction for the synthesis of (*E*)-2-(3-oxo-3-phenylprop-1-en-1-yl)-3-phenylquinazolin-4(3*H*)-one derivatives. This novel methodology facilitates the coupling of methyl ketones with 2-methyl-3-arylquinazolin-4(3*H*)-ones under mild conditions, delivering high selectivity and excellent yields. The reaction offers a significant advancement in constructing highly conjugated systems, providing a streamlined and sustainable alternative to traditional synthetic approaches. Beyond the innovative chemistry, the synthesized compounds demonstrated agonistic activity for TLX, an orphan nuclear receptor crucial for neural stem cell proliferation, development, and disease. These findings highlight the dual importance of the methodology in enabling sustainable synthesis and the biological relevance of the resulting compounds as potential therapeutic tools.

Introduction

Quinazolinones are bicyclic nitrogen-containing heterocyclic compounds characterized by a fused pyrimidine ring system at the 4′ and 8′ positions of the benzene ring. These compounds have attracted considerable attention in organic and medicinal chemistry due to their broad spectrum of pharmacological activities.[1–5] Quinazolinone heterocycles play a crucial role in various biological processes and have been widely recognized for their therapeutic potential, demonstrating antihypertensive, antimicrobial, anti-hyperlipidemic, anti-inflammatory, and anti-convulsant activities.[6,7] Furthermore, several quinazolinone derivatives have been investigated for their antitumor chemotherapeutic properties.[8,9]

Natural quinazolinone-based compounds exhibit remarkable physiological activities. For instance, rutaecarpine (**1**), a natural alkaloid, has been found to inhibit cyclooxygenase-2 (COX-2), thereby exerting anti-inflammatory effects.[10–12] Similarly, luotonin A (**2**), another quinazolinone-containing alkaloid, has demonstrated cytotoxic activity against the murine leukemia P338 cell line.[13,14] The β-indoloquinazolinone alkaloid bouchardatine (**3**) has been identified as a potential adipogenesis inhibitor, highlighting its role in metabolic regulation.[15] Moreover, the quinazolinone-based drug idelalisib (**4**) has been approved for the treatment of chronic lymphocytic leukemia (CLL).[16–18] Additionally, norquinadoline A (**5**) exhibits antiviral activity and cloroqualone (**6**) act as antitussive, further emphasizing the therapeutic significance of quinazolinone derivatives in drug discovery and development.[19]

In addition to these promising compounds, a diverse array of natural and synthetic quinazolinone derivatives has demonstrated a wide range of biological activities, including anticonvulsant, antidiabetic, sedative, and analgesic properties. These multifaceted pharmacological effects further underscore the therapeutic versatility of quinazolinone-based compounds. Fig. 1 highlights some notable examples of quinazolinone derivatives with significant medicinal potential.[1]

Quinazolin-4(3*H*)-one derivatives constitute a privileged class of nitrogen-containing heterocycles, known for their diverse pharmacological profiles. Among these, 2-methyl-3-arylquinazolin-4(3*H*)-ones have garnered considerable attention due to the synthetic versatility conferred by the reactive C-2 methyl group and the electronic tunability of the C-3 aryl moiety. These scaffolds serve as valuable intermediates in the

[a]*Department of Anesthesiology, Washington University in St Louis, St Louis, MO, USA. E-mail: belgendy@wustl.edu*
[b]*Center for Clinical Pharmacology, Washington University School of Medicine and University of Health Sciences and Pharmacy, St Louis, MO 63110, USA*
[c]*Department of Pharmaceutical and Administrative Sciences, University of Health Sciences and Pharmacy, St Louis, MO 63110, USA*
[d]*University of Florida Genetics Institute, University of Florida School of Medicine, Gainesville, FL, USA*
[e]*University of Florida College of Pharmacy, Department of Cellular and Systems Pharmacology, Gainesville, FL, USA*

† Electronic supplementary information (ESI) available. See DOI: https://doi.org/10.1039/d5ob00672d

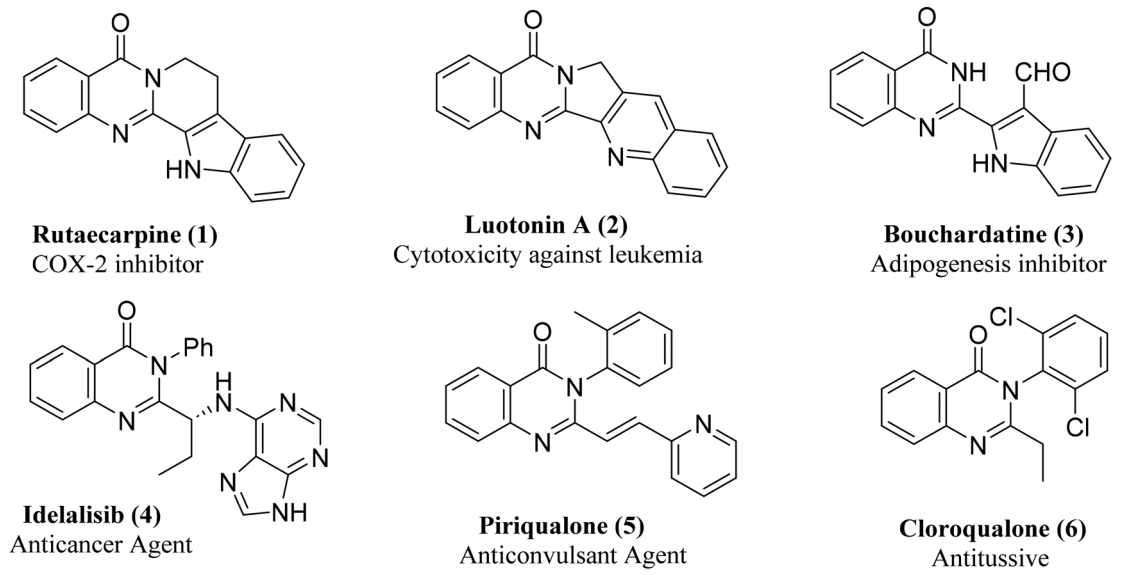

Fig. 1 Representative examples of natural and synthetic quinazolinone derivatives with therapeutic potential.

synthesis of structurally complex and biologically active compounds. Recent advances have showcased their utility in a variety of synthetic transformations, including annulation, condensation, and oxidative processes. Notably, Wang and co-workers developed a green electrochemical approach for the dual C(sp^3)–H amination of 2-methyl-3-arylquinazolin-4(3*H*)-ones, yielding imidazo-fused quinazolinones under metal- and oxidant-free conditions (Scheme 1a).[20] Complementary work by Kamal *et al.* introduced an iodine-mediated oxidative protocol that enabled the formation of fused imidazo[1,5-*a*]quinazolinones *via* condensation with benzylamines under similarly mild conditions (Scheme 1b).[21]

These quinazolinone derivatives have also shown promise in antiviral research. Song and co-workers synthesized novel heterocyclic scaffolds *via* condensation with heteroaryl aldehydes, demonstrating potent activity against Zika and Dengue viruses.[22] Zhu's group further expanded the structural diversity of these systems through a one-pot cascade reaction involving nitration and annulation, affording isoxazole-fused tricyclic alkaloids *via* concurrent C–N, C–C, and C–O bond formations (Scheme 1c). This transformation also allowed for late-stage functionalization of complex natural products.[23]

Additional noteworthy strategies include Han's Knoevenagel–Friedel–Crafts sequence to access N-heteropolycyclic quinazolinones (Scheme 1d),[24] and Charushina's synthesis of photoluminescent styrene-substituted derivatives for optoelectronic applications (Scheme 1e).[25] Basyouni's group contributed iodinated derivatives bearing pharmacophores such as thiosemicarbazones, pyrazoles, and azomethines; however, their reliance on SeO_2 for oxidation presents environmental and safety concerns.[26]

Hybrid molecules such as quinazolinone-chalcones have also demonstrated promising anti-inflammatory and antimicrobial potential. Nevertheless, the synthesis of these conjugates remains synthetically challenging due to limitations in existing methodologies. Starikova's group addressed this by employing benzils under perfluorophenol solvent conditions to yield chalcone-type derivatives (Scheme 1f).[27] Meanwhile, the widely used condensation of 2-methyl-3-arylquinazolin-4(3*H*)-ones with phenylglyoxal in acetic anhydride provides functionalized frameworks with interesting bioactivities (Scheme 1g).[28,29]

However, many current methods suffer from drawbacks such as the use of toxic oxidants like selenium dioxide and reliance on costly or less accessible reagents like phenylglyoxal. These limitations have prompted the development of a more sustainable and broadly applicable protocol employing benign and readily available reagents such as acetophenone and iodine, offering an efficient route to chalcone-type quinazolinone hybrids under environmentally friendly conditions.

In recent years, metal-free catalyzed oxidative C–H functionalization strategies have garnered significant attention due to their cost-effectiveness and environmentally benign byproducts.[30–32] Among these, molecular iodine, known for its multiple oxidation states and mild redox potential, has been widely employed in oxidative coupling reactions.[33–35] Additionally, iodine/DMSO-mediated oxidative coupling reactions have been explored to a certain extent, demonstrating their synthetic versatility.[36–45]

Despite considerable progress in the field, the direct catalytic transformation of heterocycles *via* an iodine-catalyzed approach remains a promising yet underexplored area. Building on our previous work in developing synthetic methodologies to facilitate the synthesis of scaffolds important in medicinal chemistry,[46–51] as well as relevant literature reports,[28] we herein present an I_2-catalyzed cross-coupling strategy for the synthesis of 4(3*H*)-quinazolinone chalcone derivatives. This approach aligns with our ongoing efforts to expand efficient and versatile synthetic routes for bioactive

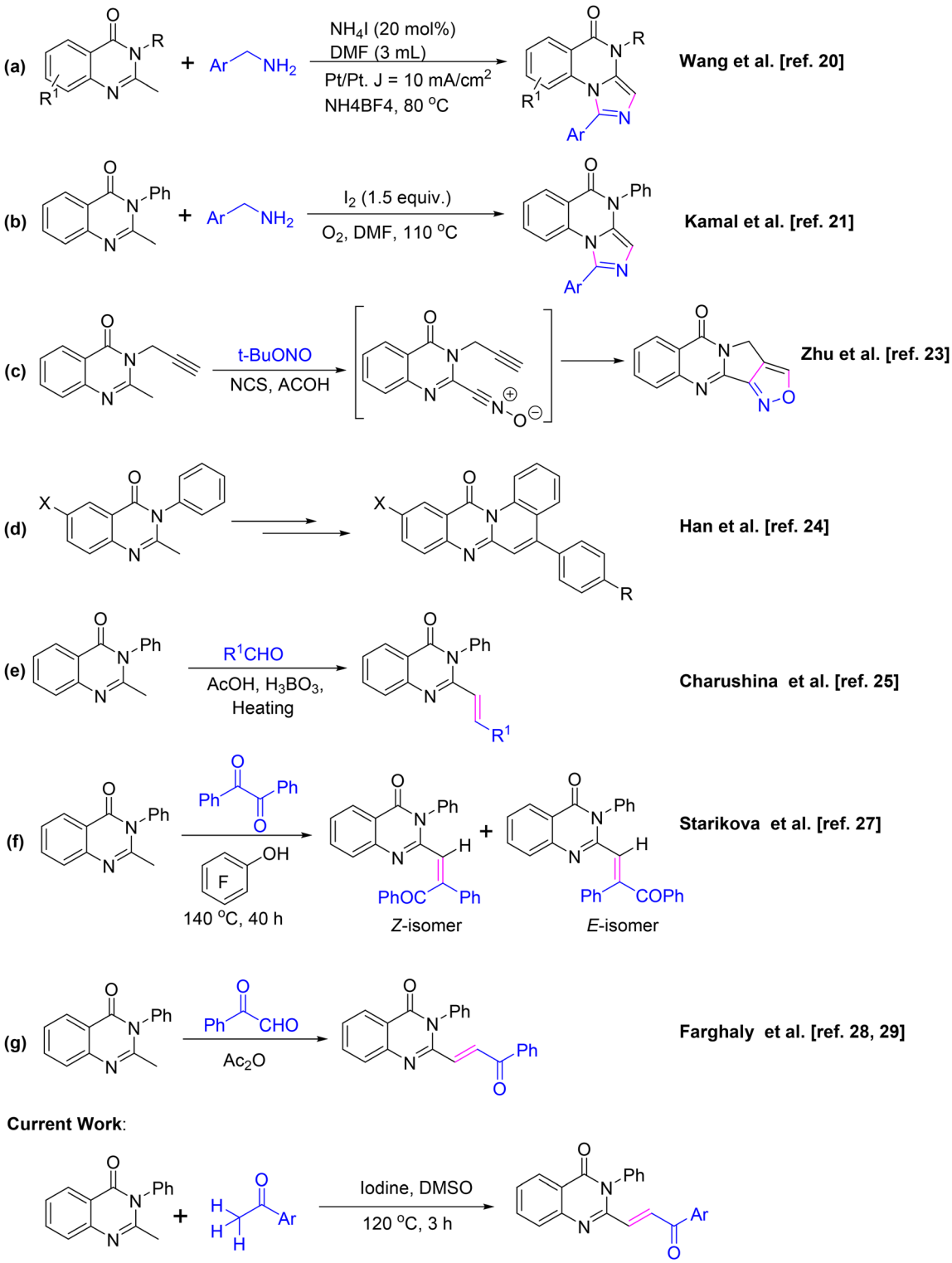

Scheme 1 Synthesis of quinazolin-4(3*H*)-one derivatives, highlighting both previous and current work.

heterocyclic frameworks. This transformation proceeds through an oxidative C(sp^3)–H activation followed by a condensation process, offering an efficient and sustainable route to privileged heterocyclic frameworks.

TLX is an orphan nuclear receptor with a pivotal role in neural stem cell proliferation.[52–54] A homolog of the Drosophila tailless (tll) gene, TLX possesses a well-defined ligand-binding domain (LBD), making it a promising drug-

gable target despite the absence of broadly accepted endogenous ligand. It is predominantly expressed in neurogenic regions of the brain, such as the subventricular zone and the sub granular zone, where it promotes neurogenesis *via* direct gene regulation. Through its regulatory influence on genes such as PTEN, p21/CDKN1A, and VEGF, TLX orchestrates key processes including cell cycle progression, senescence, and angiogenesis. Given its fundamental role in neurogenesis and its implication in various cancers such as glioblastoma, TLX emerges as an attractive therapeutic target, particularly for the development of synthetic ligands that could modulate its activity for clinical applications.

Previously, we identified BMS453 (7) and BMS493 (**8**) (Fig. 2) as efficacious TLX agonists that were able to substantially enhance gene repression by TLX.[55] Building on the promising characteristics of 2-(α,β-unsaturated ketone)-3-phenylquinazolin-4(3*H*)-ones and their structural resemblance to BMS453 and BMS493, we developed 4(3*H*)-quinazolinone-based chemical probes targeting TLX. By leveraging a straightforward and efficient C–H activation strategy, our approach aimed to facilitate the synthesis of functionalized 4(3*H*)-quinazolinones. This will enable a deeper investigation into their potential as selective modulators of TLX activity, expanding opportunities for therapeutic intervention.

Results and discussion

As part of our ongoing efforts to develop efficient methodologies for the synthesis of novel heterocyclic scaffolds, we initiated our investigation using 2-methyl-3-phenylquinazolin-4(3*H*)-one (**9a**) and acetophenone (**10**) as a model system. This system served as a platform for both optimization and mechanistic exploration. The results of our condition screening are summarized in Table 1.

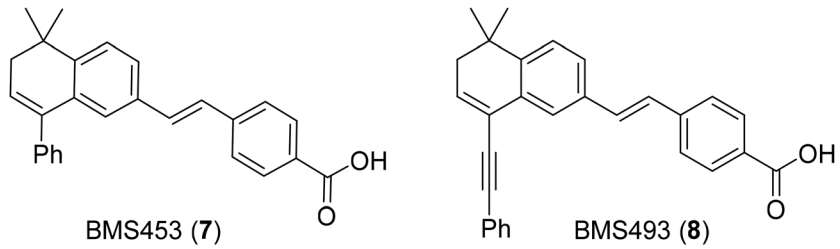

Fig. 2 TLX agonists BMS453 (7) and BMS493 (**8**).

Table 1 Optimization of reaction conditions[a]

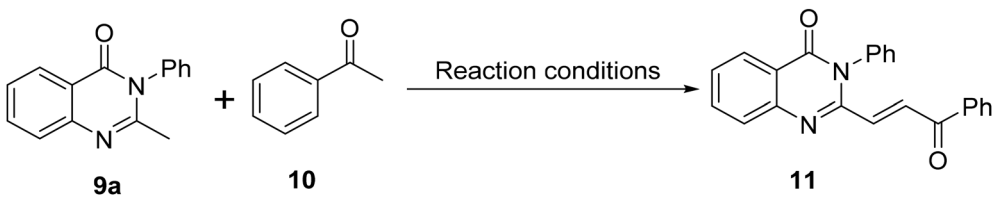

Entry	Catalyst (equiv.)	Solvent	Temperature (°C)	Yield[b] (%)
1	Iodine (0.2)	Toluene	100 °C	NR
2	Iodine (0.2)	DMF	100 °C	NR
3	Iodine (0.2)	DMA	100 °C	NR
4	Iodine (0.2)	CH_3CN	90 °C	NR
5	Iodine (0.2)	DMSO	80 °C	NR
6	Iodine (0.2)	DMSO	90 °C	Trace
7	Iodine (0.2)	DMSO	100 °C	40
8	Iodine (0.5)	DMSO	120 °C	65
9	Iodine (1.0)	DMSO	120 °C	90
10	Iodine (1.5)	DMSO	120 °C	75
11	—	DMSO	120 °C	NR
12	KI (1.0)	DMSO	120 °C	NR
13	NIS (1.0)	DMSO	120 °C	10
14	TBAI (1.0)	DMSO	120 °C	NR
15	NH_4I (1.0)	DMSO	120 °C	NR

[a] Reaction conditions: **9** (1.0 equiv.), **10** (3.0 equiv.), I_2 catalyst (1.0 equiv.) and solvent (4 mL) are heated in a sealed tube at 120 °C for 3 h. [b] Yield of the isolated product. DMF = *N*,*N*-dimethyl formamide, DMA = *N*,*N*-dimethylacetamide, CH_3CN = acetonitrile, DMSO = dimethyl sulfoxide. The reactions were carried out in a sealed tube under air, without the use of an inert atmosphere (Ar or N_2), by combining the reactants with iodine or an alternative promoter in DMSO as the solvent.

Initial experiments revealed that treatment of **9a** and **10** with 20 mol% molecular iodine (I_2) in DMSO at 100 °C afforded the desired product **11** in 40% yield (Table 1, entry 7). Encouraged by this outcome, we performed a comprehensive optimization of the reaction conditions, including variation of solvent, temperature, and iodine loading. DMSO emerged as the most effective solvent, and increasing the I_2 loading to 100 mol% while elevating the temperature to 120 °C significantly enhanced the product yield to 90% (entry 9).

The structure of product **11** was confirmed by NMR spectroscopy. The stereochemistry of the newly formed olefinic bond was unambiguously assigned as *E* based on the diagnostic coupling constant (J > 14 Hz) observed in the ^{1}H NMR spectrum.

To further probe the catalytic role of iodine, a range of iodine sources was evaluated. *N*-Iodosuccinimide (NIS) delivered only a 10% yield of **11** (entry 13), while other iodide salts, including KI, TBAI, and NH_4I (entries 12, 14, and 15), failed to promote the transformation. Notably, both sub-stoichiometric and supra-stoichiometric amounts of I_2 (entries 8 and 10) led to diminished yields, underscoring the critical role of optimal iodine concentration for efficient conversion.

With the optimized reaction conditions in hand (Table 1, entry 7), we extended our investigation to various aryl methyl ketones, as illustrated in Scheme 2. Aryl methyl ketones bearing electron-donating and electron-withdrawing groups were successfully converted into their corresponding quinazolinone derivatives in moderate to excellent yields (66–92%, **11–43**). Additionally, sterically hindered acetyl naphthalene exhibited only a slight impact on reaction efficiency, affording **28** (BE4160) in 60% yield. Notably, heterocyclic methyl ketones also participated effectively, yielding the desired product **30** (BE4131) in 85% yield, further demonstrating the broad substrate scope and synthetic applicability of this iodine-catalyzed oxidative cross-coupling strategy.

To gain deeper insight into the reaction mechanism, a series of controlled experiments were conducted (Scheme 3). Initially, we examined whether the reaction could proceed in the absence of iodine (as a promoter) or DMSO. When compound **9a** was reacted with **10** at 120 °C for 3 hours under these conditions, no formation of product **11** was observed (Scheme 3A).

In the second controlled experiment, we investigated whether the reaction proceeds *via* the formation of a corresponding aldehyde intermediate from **9a**. To test this, compound **9a** was treated with iodine in DMSO at 120 °C for 3 hours (Scheme 3B). TLC analysis showed complete consumption of **9a**, with the appearance of multiple spots; however, LC-MS analysis did not reveal the formation of any aldehyde intermediate. Furthermore, the subsequent addition of acetophenone to the reaction mixture did not lead to the formation of product **11**, suggesting that an aldehyde intermediate was not involved.

In a third controlled experiment, acetophenone (**10**) was reacted with iodine in DMSO at 120 °C for 2 hours. LC-MS analysis confirmed the formation of a phenylglyoxal intermediate. Upon addition of **9a** to this reaction mixture and stirring for an additional hour, the desired product **11** was obtained in 80% yield (Scheme 3C). Based on these observations, we hypothesize that molecular iodine (I_2) facilitates the iodination of acetophenone to form an α-iodoacetophenone intermediate, which is subsequently oxidized by DMSO to generate phenyl-

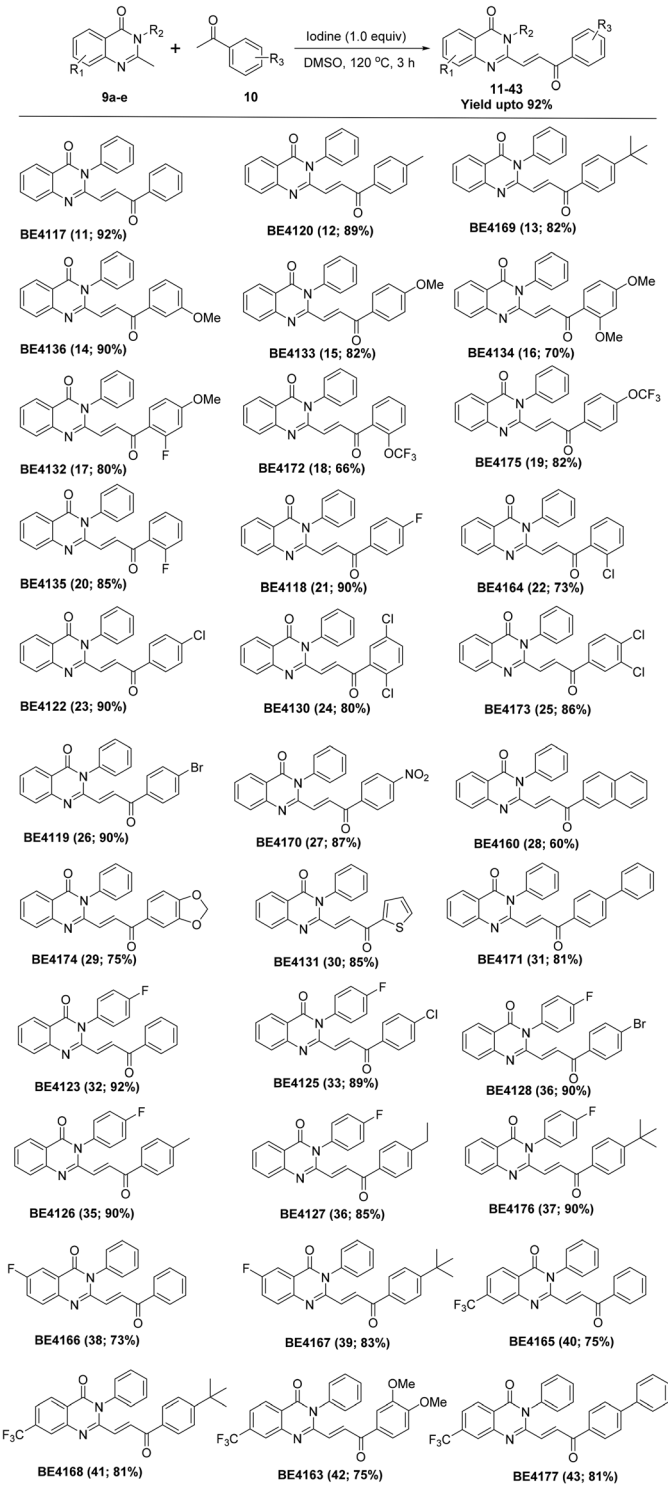

Scheme 2 Iodine-catalyzed cross-coupling synthesis of quinazolinone derivatives: substrate scope and yields (**11–43**). Reactions were carried out with **9** (1.0 mmol), **10** (3.0 mmol), iodine (1.0 equiv.) in DMSO (4.0 mL) in a sealed tube at 120 °C for 3 h.

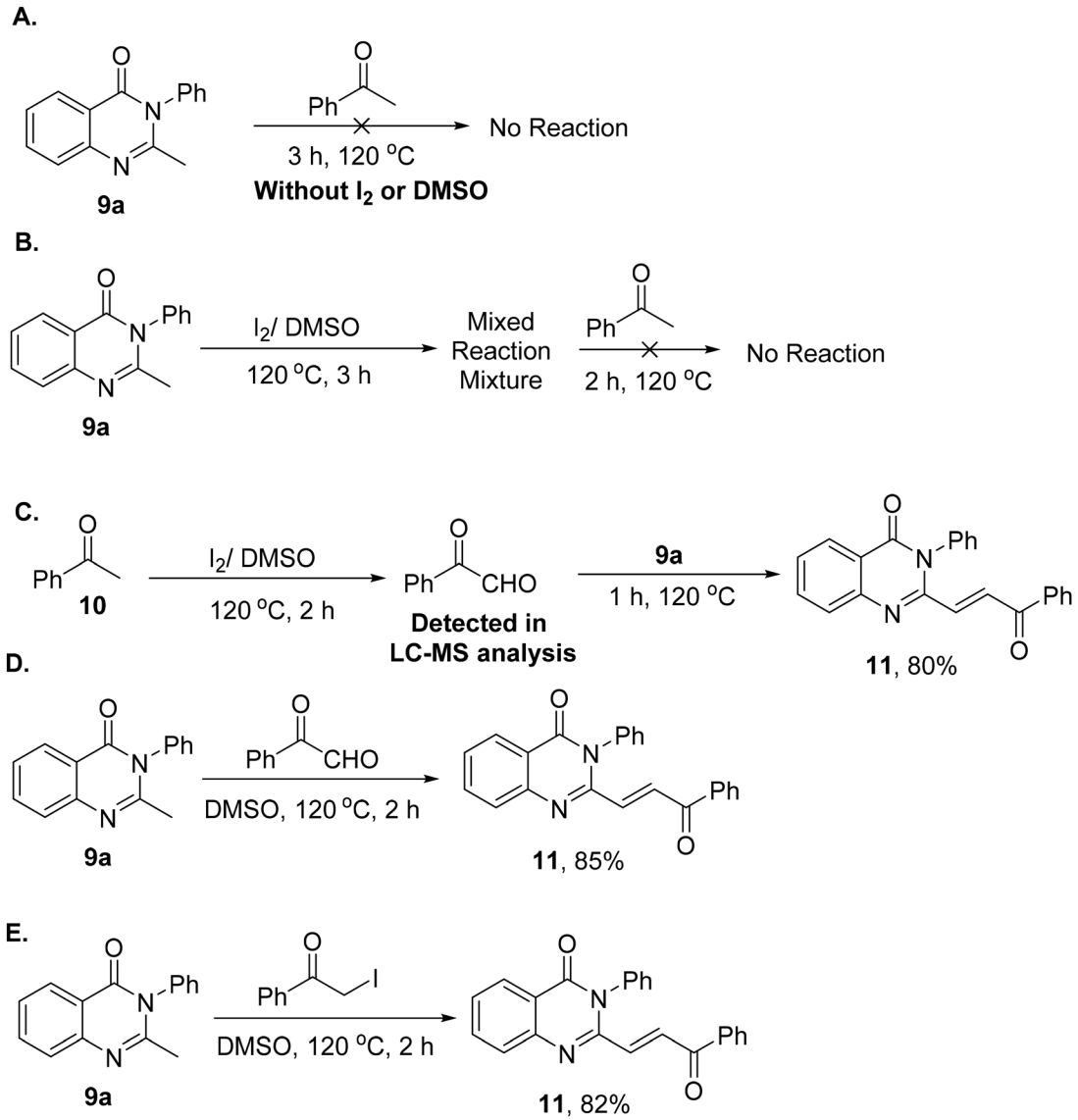

Scheme 3 Mechanistic investigation of the iodine-promoted cross-coupling reaction.

glyoxal. The *in situ* generated phenylglyoxal then undergoes condensation with quinazolinone **9a**, yielding the target compound **11**.

To validate this hypothesis, the model reaction was carried out in the absence of DMSO or iodine, under which no product formation was observed, confirming their essential roles in the transformation. Furthermore, when the reaction was performed using phenylglyoxal and DMSO without an iodine catalyst, the formation of **11** was still observed (Scheme 3D). Additionally, another experiment was conducted by reacting quinazolinone (**9a**) with α-iodoacetophenone in DMSO, which also successfully led to the formation of **11** (Scheme 3E).

These findings strongly indicate that molecular iodine and DMSO play a crucial role in the reaction mechanism, supporting the proposed pathway involving sequential α-iodination, oxidation, and condensation steps.

Based on these experimental results and previous reports,[56] a possible mechanism for the oxidative cross-coupling reaction is illustrated in Scheme 4. Initially, the methyl ketone **10** reacts with molecular iodine, yielding α-iodoacetophenone (**10aa**), which undergoes oxidation by DMSO to form phenylglyoxal (**10ab**). This intermediate then participates in an addition reaction, forming a C–C bond (**10ac**). Subsequent dehydration leads to the final product **11**. The reaction is proposed to proceed *via* a cascade sequence involving C–H functionalization, oxidation, and C–C bond formation.

Biological activity

The activity of TLX was evaluated through a ligand-sensing assay designed to measure whether a potential ligand can trigger a conformational shift in the ligand-binding domain of TLX, thereby promoting the recruitment of a transcriptional coactivator protein. This assay has been effectively employed

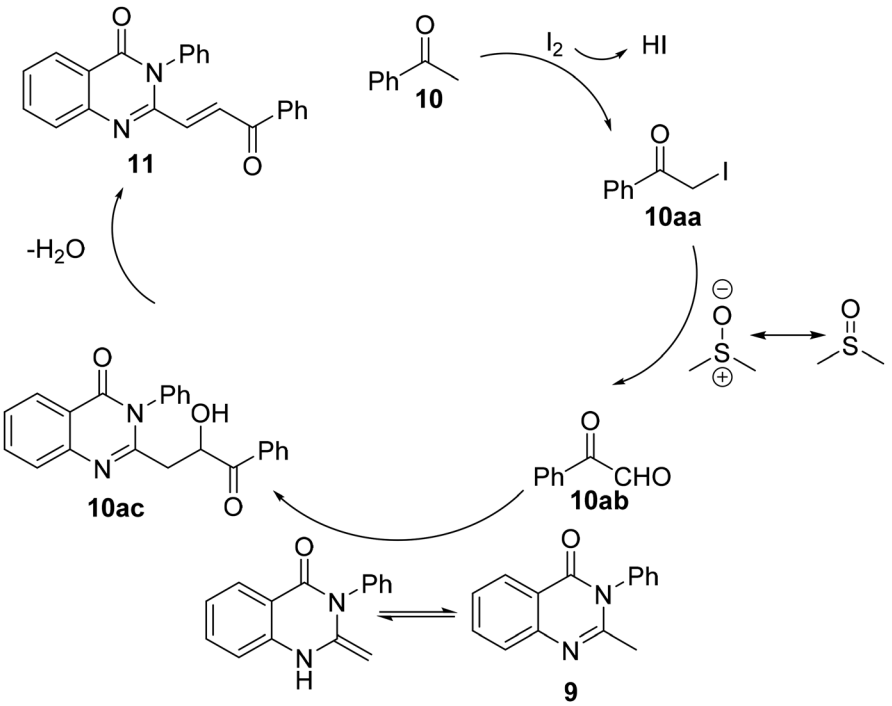

Scheme 4 Proposed mechanism for the synthesis of (*E*)-2-(3-oxo-3-phenylprop-1-en-1-yl)-3-phenylquinazolin-4(3*H*)-one.

to identify ligands such as retinoids and oleic acid as ligands for TLX.[57–59] Oleic acid demonstrated a potency of 4.456 μM in this assay and facilitated recruitment of NR box peptide derived from the nuclear receptor-interacting protein 1 (NR1P1; receptor-interacting protein 140 (RIP140) transcriptional cofactor). Many compounds showed improved potency and efficacy in recruiting RIP140 when compared to oleic acid (Table 2).

To gain initial insights into the structure–activity relationship (SAR) of the chalcone-quinazolinone scaffold as TLX agonists, we conducted a preliminary exploration of modifications at key regions of the molecule. By introducing selected electronic, steric, and lipophilic substitutions at both the chalcone phenyl ring and the quinazolinone core, we aimed to identify early trends in activity and establish a foundation for further optimization rather than an exhaustive SAR analysis.

The SAR analysis of the phenyl ring within the chalcone moiety reveals key trends influenced by electronic effects, steric hindrance, and lipophilicity. The unsubstituted phenyl ring showed a modest increase in potency and reduced efficacy

Table 2 Evaluation of synthesized compounds as ligands to TLX

Entry	Compound	EC_{50} (μM)	E_{max} (%)	Entry	Compound	EC_{50} (μM)	E_{max} (%)
1	**Oleic acid**	**4.909**	**100.0**[a]	18	BE4170 (**27**)	1.897	107.9
2	BE4117 (**11**)	4.231	94.4	19	BE4160 (**28**)	16.922	158.5
3	BE4120 (**12**)	5.052	94.8	20	BE4174 (**29**)	8.886	125.5
4	BE4129 (**13**)	5.721	105.6	21	BE4131 (**30**)	4.989	117.1
5	BE4136 (**14**)	6.672	110.2	22	BE4171 (**31**)	1.662	103.1
6	BE4133 (**15**)	3.761	97.7	23	BE4123 (**32**)	7.005	92.6
7	BE4134 (**16**)	3.746	95.4	24	BE4125 (**33**)	6.275	122.9
8	BE4132 (**17**)	1.786	111.2	25	BE4128 (**34**)	3.657	114.1
9	BE4172 (**18**)	8.695	106.3	26	BE4126 (**35**)	3.811	80.6
10	BE4175 (**19**)	7.912	108.2	27	BE4127 (**36**)	3.421	105.7
11	BE4135 (**20**)	16.948	124.9	28	BE4176 (**37**)	2.415	122.0
12	BE4118 (**21**)	5.29	85.3	29	BE4166 (**38**)	10.714	128.5
13	BE4164 (**22**)	7.543	123.1	30	BE4167 (**39**)	3.266	128.2
14	BE4122 (**23**)	2.066	110.8	31	BE4165 (**40**)	3.651	134.1
15	BE4130 (**24**)	1.866	121.0	32	BE4168 (**41**)	1.676	133.3
16	BE4173 (**25**)	1.69	129.1	33	BE4163 (**42**)	4.317	121.9
17	BE4119 (**26**)	4.952	120.1	34	BE4177 (**43**)	0.468	109.8

[a] Activity of oleic acid is set to 100%.

compared to oleic acid (BE4117, EC_{50} = 4.231 μM, E_{max} = 94.1%). Introduction of alkyl substituents at the *para*-position led to diminished potency. A *para*-methyl group slightly decreased activity (BE4120, EC_{50} = 5.052 μM), while the bulkier *para-tert*-butyl group had an even greater negative impact (BE4129, EC_{50} = 5.721 μM), suggesting that increased lipophilicity and steric bulk are unfavorable at this position.

Methoxy substitutions produced variable effects. A *meta*-methoxy group reduced potency (BE4136, EC_{50} = 6.672 μM), whereas a *para*-methoxy group improved it (BE4133, EC_{50} = 3.761 μM). A 2,4-dimethoxy substitution yielded comparable potency (BE4134, EC_{50} = 3.746 μM) and efficacy (E_{max} = 95.4%). Notably, the combination of an *ortho*-fluoro and *para*-methoxy group (BE4132, EC_{50} = 1.786 μM, E_{max} = 111.2%) significantly enhanced both potency and efficacy, indicating a synergistic interaction possibly arising from electron-donating and halogen-bonding effects. Conversely, trifluoromethoxy substitutions at the *ortho* (BE4172) and *para* (BE4175) positions resulted in substantial activity loss, likely due to steric clashes or unfavorable electronic properties.

Fluorine substitutions were generally detrimental. An *ortho*-fluoro group severely decreased activity (BE4135, EC_{50} = 16.948 μM), and a *para*-fluoro group only retained weak agonist activity (BE4118, EC_{50} = 5.29 μM). Similar trends were observed with halogen substitutions: *ortho*-chloro (BE4164, EC_{50} = 7.543 μM) and *para*-bromo (BE4119, EC_{50} = 4.952 μM) reduced potency. In contrast, electron-withdrawing and hydrophobic halogen substituents at specific positions enhanced activity: *para*-chloro (BE4122, EC_{50} = 2.066 μM), *para*-nitro (BE4170, EC_{50} = 1.897 μM), 2,5-dichloro (BE4130, EC_{50} = 1.866 μM), and 3,4-dichloro (BE4173, EC_{50} = 1.690 μM). These improvements are likely driven by favorable π-stacking and hydrophobic interactions in the binding site.

Fused ring systems like β-naphthyl (BE4160) and benzo[*d*][1,3]dioxole (BE4174) led to significant potency loss, suggesting that increased planarity or steric bulk disrupts optimal binding. However, a thiophene ring replacement showed comparable activity to the phenyl ring and OA (BE4131, EC_{50} = 4.989 μM). Remarkably, a 1,1′-biphenyl system significantly enhanced potency (BE4171, EC_{50} = 1.662 μM), highlighting the binding site's tolerance or preference for extended aromatic ring system.

Modifications at the quinazolinone core in conjunction with phenyl chalcone substitutions further elucidated SAR features. A *para*-fluoro substitution at position 3 of the quinazolinone ring (BE4123, EC_{50} = 7.005 μM) reduced potency relative to the unsubstituted BE4117. When combined with phenyl chalcone modifications, activity varied: *para*-chloro (BE4125, EC_{50} = 6.275 μM) improved activity modestly, while *para*-bromo (BE4128, EC_{50} = 3.657 μM) showed greater potency than the non-fluorinated counterpart (BE4119, EC_{50} = 4.952 μM), indicating additive benefits of halogen pairing.

Alkyl substitutions at the *para*-position of the phenyl chalcone ring correlated with increased potency as bulk increased: *p*-Me (BE4126, EC_{50} = 3.811 μM), *p*-Et (BE4127, EC_{50} = 3.421 μM), and *p-t*-Bu (BE4176, EC_{50} = 2.415 μM). These results underscore the importance of hydrophobic volume at this position in enhancing receptor binding.

Interestingly, fluorine substitution at position 6 of the quinazolinone core (BE4166, EC_{50} = 10.714 μM) failed to improve activity. However, when paired with a *p-t*-Bu group on the phenyl chalcone ring, potency significantly improved (BE4167, EC_{50} = 3.266 μM), again emphasizing the role of steric bulk.

A trifluoromethyl group at position 7 (BE4165, EC_{50} = 3.651 μM) modestly enhanced activity, which was further improved when combined with *p-t*-Bu substitution (BE4168, EC_{50} = 1.676 μM). However, electron-donating groups such as 3,4-dimethoxy (BE4163, EC_{50} = 4.317 μM) led to decreased potency, suggesting that electron-rich environments may be less favorable at this site.

Finally, substitution with a 1,1′-biphenyl system again confirmed the benefit of extended aromaticity (BE4177, EC_{50} = 0.468 μM), reinforcing the conclusion that such structures enhance binding, possibly *via* increased π-interactions or enhanced fit within an extended hydrophobic pocket.

Overall, SAR analysis reveals that steric bulk at the *para*-position (*e.g.*, *p-t*-Bu, *p*-Cl, *p*-Br) and electron-withdrawing groups at strategic locations on the quinazolinone core substantially enhance potency. Dichlorinated derivatives and extended aromatic systems yielded the most potent analogs. Crucially, introducing fluorine or trifluoromethyl groups on the quinazolinone core, particularly at positions 6 and 7, significantly improves potency when paired with bulky hydrophobic substituents (*e.g.*, *p-t*-Bu) on the phenyl chalcone ring. The data strongly supports a binding site architecture that favors extended aromatic systems and strategically placed hydrophobic substituents for improved biological activity. These findings provide a clear strategy for optimizing chalcone-quinazolinone derivatives for improved pharmacological activity and receptor binding affinity.

Future studies will aim to further expand the structure–activity relationship (SAR) by exploring additional modifications to enhance potency and efficacy. Additionally, newly identified agonists will undergo comprehensive *in vitro* evaluation of absorption, distribution, metabolism, and excretion (ADME), pharmacokinetics (PK), and off-target effects to ensure their drug-like properties and selectivity. These efforts will provide a more complete understanding of the scaffold's potential and guide the rational design of optimized TLX agonists.

Molecular modeling of TLX ligands

The ligand-binding domain (LBD) of TLX adopts the canonical nuclear receptor architecture, characterized by a three-layered α-helical sandwich formed by helices H3 through H12. In the apo state, H12 is positioned within the coactivator-binding groove, stabilizing an autorepressed conformation. The ligand-binding pocket (LBP) is occluded by bulky hydrophobic residues and a kinked H12, preventing spontaneous ligand entry.[60] Molecular dynamics simulations revealed that the synthetic retinoid BMS493 can bind within the LBP by displacing H11, creating sufficient space to accommodate its structure.[55] The phenyl ethynyl group of BMS493 extends into a hydro-

phobic groove between H3 and H11, engaging residues F362 and F363, while the dihydronaphthalen-vinyl benzoic acid group primarily forms hydrophobic interactions with L192, L242, I230, L268, I235, and I353 (Fig. 3A).

All selected ligands exhibit molecular interaction patterns similar to those of BMS493 (Fig. 3B–H), primarily engaging the hydrophobic ligand-binding pocket (LBP) of TLX. A key distinguishing feature among these compounds is the presence

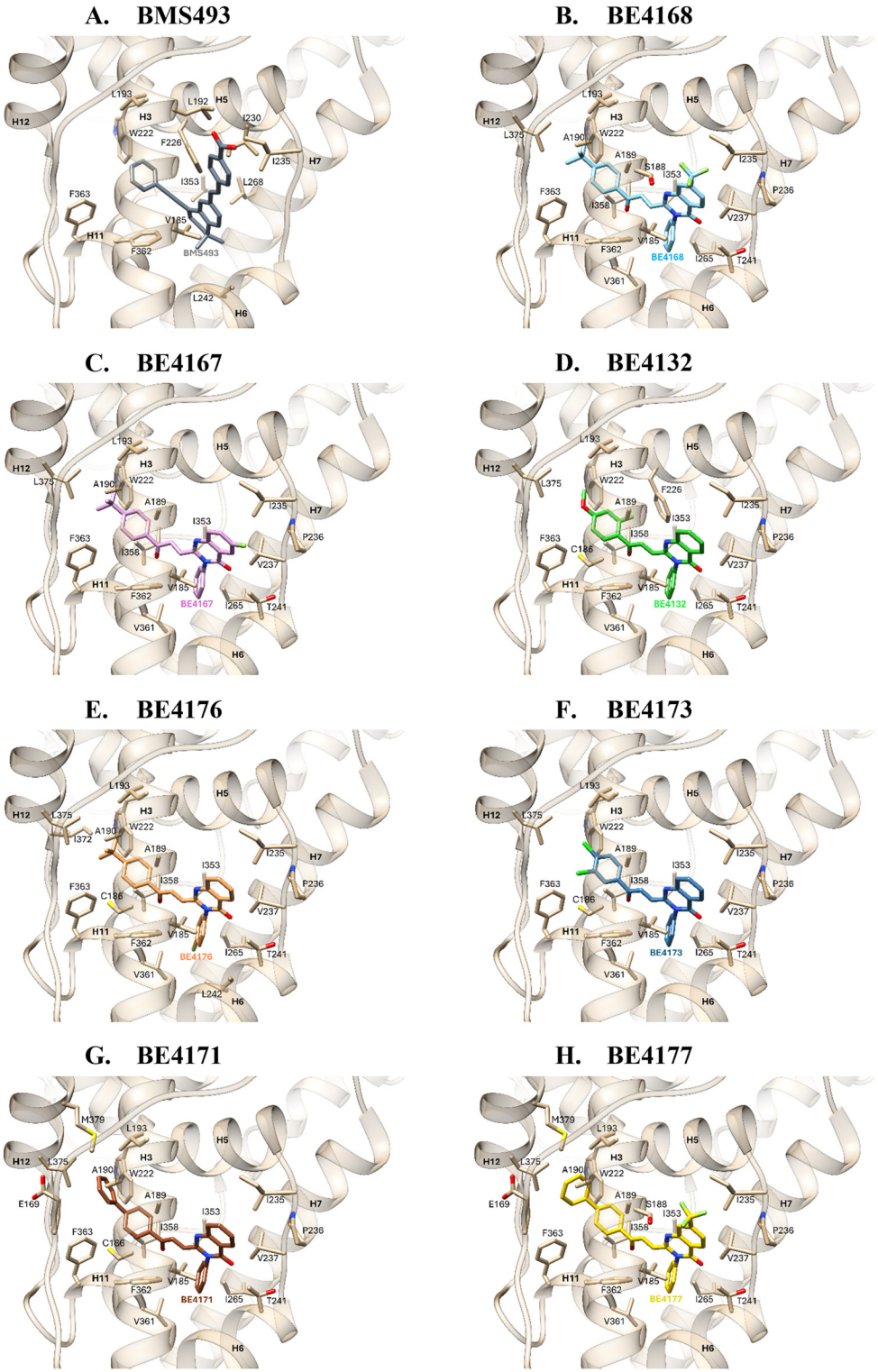

Fig. 3 Binding poses and molecular interactions of ligands in TLX LBP: A. BMS493. B. BE4168. C. BE4167. D. BE4132. E. BE4176. F. BE4173. G. BE4171. H. BE4177.

of a chalcone moiety, which penetrates more deeply into the binding pocket than BMS493. This deeper insertion enables extended hydrophobic interactions with helices H3, H11, and H12, including residues within H12 that are not contacted by BMS493. Additionally, all ligands possess a quinazolinone core that consistently mediates key interactions with residues V185, P236, V237, and T241. This core establishes electrostatic interaction with the backbone of P236 and engage in hydrophobic contacts with I235 and V185. Notably, its carbonyl group forms electrostatic interactions with V237 and T241, while the amine moiety contributes to binding *via* interaction with V185. Collectively, these coordinated interactions enhance both the stability and specificity of the ligand–receptor complex.

Notable variations in ligand binding arise from differences in specific substituents across the compound series. For example, the $-CF_3$ group at the 6-position of the quinazolinone ring in BE4168 (Fig. 3B) and BE4177 (Fig. 3H) promotes interaction with residue S188—an interaction not observed in BE4167 (Fig. 3C), where a single fluorine atom at the same position fails to engage this residue. BE4132 (Fig. 3D) demonstrates a unique electrostatic interaction between its *ortho*-fluorine and F226, whereas BE4176 (Fig. 3E) features a fluorophenyl group that forms electrostatic contact with L242, a feature absents in both BE4132 and BE4173 (Fig. 3F). In BE4173, replacing the *para*-*t*-butyl group seen in BE4167 with a dichloro substitution abolishes interaction with A190 but retains hydrophobic interactions with residues C186, L193, F363, and L375.

Particularly noteworthy are BE4171 and BE4177, which possess an extended chalcone phenyl group, exhibit enhanced hydrophobic interactions with residues E169, L375, and M379 as the group penetrates deeper into the binding groove formed by H3, H12, and T155-E179 loop (Fig. 3E and H). These structural variations illustrate how subtle chemical modifications can significantly influence binding specificity and affinity, emphasizing the adaptability of the scaffold for targeted engagement with the TLX ligand-binding pocket.

Conclusion

In conclusion, we demonstrated the successful development of a highly efficient iodine-catalyzed oxidative cross-coupling reaction for the synthesis of (*E*)-2-(3-oxo-3-phenylprop-1-en-1-yl)-3-phenylquinazolin-4(3*H*)-one derivatives. This innovative approach showcases the power of C–H activation strategies in constructing complex and highly conjugated systems with excellent yields, regioselectivity, and functional group tolerance. The streamlined methodology not only provides a sustainable and versatile platform for the functionalization of 4(3*H*)-quinazolinones but also highlights the potential of iodine catalysis in advancing synthetic organic chemistry. These advances underscore the broad applicability of this reaction in the development of bioactive molecules as TLX receptor agonists, including chemical tools for exploring nuclear receptor biology, thereby bridging the gap between synthetic chemistry and medicinal applications.

Preliminary structure–activity relationship (SAR) studies revealed key modifications that enhance potency, including *para*-halogenation (*p*-Cl, *p*-Br) on the phenyl chalcone ring and fluorine or trifluoromethyl substitutions on the quinazolinone core. Notably, *para*-fluoro substitution on the quinazolinone core synergistically enhanced the effect of halogenation at the phenyl chalcone ring, demonstrating a strategic approach to improving receptor binding affinity. Additionally, increasing steric bulk through alkyl groups (*p*-Me, *p*-Et, *p*-*t*-Bu) at the phenyl chalcone ring correlated with enhanced activity, further guiding the optimization of this scaffold. These findings lay the groundwork for the rational design of next-generation TLX agonists, with future efforts focused on expanding SAR, improving pharmacokinetic properties (ADME, PK), and assessing off-target effects to advance these molecules toward therapeutic applications.

In summary, SAR and molecular modeling studies reveal that TLX modulation is enhanced by *para*-substituted bulky groups on the chalcone ring and electron-withdrawing substituents, especially fluorine and trifluoromethyl groups, on the quinazolinone core. The most potent ligands feature dichlorinated or extended aromatic systems that engage key hydrophobic regions of the TLX ligand-binding pocket. Notably, extended chalcone phenyl groups, as seen in BE4171 and BE4177, further strengthen receptor interactions. These findings provide a clear framework for designing next-generation TLX agonists with improved potency and selectivity. Ongoing efforts will focus on expanding SAR around this versatile scaffold, while *in vitro* characterization of ADME properties, pharmacokinetics, and off-target profiles will guide optimization toward drug-like candidates with therapeutic potential.

Experimental section

General methods

All materials were purchased from commercial suppliers and used without further purification. The purities of the final compounds were characterized by high-performance liquid chromatography (LC/MS) using a gradient elution program (Ascentis Express Peptide C18 column, acetonitrile/water 5/95/95/5, 5 min, 0.05% formic acid) and UV detection (254 nM). The purities of the final compounds were 95% or greater. Microwave experiments were performed using Biotage Initiator +. These reactions were performed in standard Biotage Microwave Reaction Vials (10–20 mL), and the reaction mixture was stirred by a magnetic stirring bar inside the microwave reaction vial. The desired temperature was set and monitored from the instrument's 10.4″ touch screen. Temperature cannot exceed 250 °C as higher temperature cannot be used with 10–20 mL vials in solvent-free reactions as recommended by the manufacturer. All the reactions were performed in sealed vials, and there was no pressure build-up during the reaction. After processing, the reaction mixture is immediately cooled with pressurized air. The reaction is heated through high-frequency microwaves (2.45 GHz), generated by magnetron.

Melting points of the compounds were recorded with Reach Devices (RD-MP) digital melting point determination apparatus. NMR spectra were recorded on a Bruker NMR 400 MHz Avance III spectrometer operating at 400 MHz for ^{1}H NMR and 100 MHz for ^{13}C NMR. Chemical shifts are given in part per million (ppm) relative to tetramethyl silane (TMS) and coupling constants J are given in Hertz. HRMS analysis was conducted at Old Dominion University COSMIC using positive-ion mode electrospray ionization (ESI) in an Apollo II ion source, mounted on a high-field Bruker 10 Tesla with SolariX XR Hybrid FTICR FT ICR mass spectrometer.

General procedure for oxidative cross-coupling for the synthesis of (*E*)-2-(3-oxo-3-phenylprop-1-en-1-yl)-3-phenylquinazolin-4(3*H*)-one by C–H activation

To a stirred solution of 2-methyl-3-phenylquinazolin-4(3*H*)-one (**9a**; 100.0 mg, 0.42 mmol, 1.0 equiv.) and acetophenone (152.49 mg, 1.27 mmol, 0.148 mL, 3.0 equiv.) in DMSO (5.0 mL) was added iodine (107.37 mg, 0.42 mmol, 1.0 equiv.) at room temperature. After the addition was completed, the reaction vial was sealed with a cap, and the mixture was heated at 120 °C for 3 hours. The progress of the reaction was monitored by TLC and LC-MS analysis. Upon completion, the reaction mixture was cooled to room temperature and diluted with EtOAc (5.0 mL). The excess iodine was quenched with aqueous $Na_2S_2O_3$ (10.0 mL). The mixture was extracted with EtOAc (3 × 10 mL), washed successively with water and brine, and dried over anhydrous Na_2SO_4. After filtration, the solvent was removed under reduced pressure. The crude product was recrystallized from MeOH, yielding the pure product.

(*E*)-2-(3-Oxo-3-phenylprop-1-en-1-yl)-3-phenylquinazolin-4(3*H*)-one (BE4117; 11). Yield: 137.1 mg (92%), yellow solid; m.p. = 247.2–249.6 °C; ^{1}H NMR (400 MHz, $CDCl_3$): δ 8.41 (d, J = 8.0 Hz, 1H), 8.32 (d, J = 14.8 Hz, 1H), 8.08 (d, J = 7.7 Hz, 2H), 7.96–7.90 (m, 2H), 7.73–7.60 (m, 6H), 7.57 (t, J = 7.6 Hz, 2H), 7.42–7.31 (m, 3H), 7.13 (d, J = 14.9 Hz, 1H); ^{13}C NMR (100 MHz, $CDCl_3$): δ 189.0, 161.9, 149.9, 149.9, 147.2, 136.9, 134.8, 134.7, 133.5, 131.4, 130.1, 130.0, 129.7, 128.7, 128.6, 128.5, 127.9, 127.8, 127.8, 121.5; HRMS m/z for $C_{23}H_{17}N_2O_2$ $[M + H]^+$. Calcd 353.1284, found 353.1285.

(*E*)-2-(3-Oxo-3-(*p*-tolyl)prop-1-en-1-yl)-3-phenylquinazolin-4(3*H*)-one (BE4120; 12). Yield: 109 mg (89%), yellow solid; m.p. = 231.9–233.6 °C; ^{1}H NMR (400 MHz, $CDCl_3$): δ 8.34 (dt, J = 7.9, 1.1 Hz, 1H), 8.24 (dd, J = 15.0, 0.8 Hz, 1H), 7.92 (d, J = 8.0 Hz, 2H), 7.89–7.80 (m, 2H), 7.63–7.50 (m, 4H), 7.30 (ddd, J = 8.0, 3.2, 1.7 Hz, 4H), 7.05 (dd, J = 14.9, 0.9 Hz, 1H), 2.43 (s, 3H); ^{13}C NMR (100 MHz, $CDCl_3$): δ 188.4, 161.9, 150.1, 147.3, 144.6, 136.2, 134.8, 134.4, 134.3, 131.5, 130.1, 129.7, 129.5, 128.9, 128.5, 127.9 127.8, 127.2, 121.5, 21.7; HRMS m/z for $C_{24}H_{19}N_2O_2$ $[M + H]^+$. Calcd 367.1441, found 367.1440.

(*E*)-2-(3-(4-(*tert*-Butyl)phenyl)-3-oxoprop-1-en-1-yl)-3-phenylquinazolin-4(3*H*)-one (BE4169; 13). Yield: 147.4 mg (82%), pale yellow solid; m.p. = 209.8–210.9 °C; ^{1}H NMR (400 MHz, $CDCl_3$): δ 8.37–8.30 (m, 1H), 8.24 (d, J = 14.9 Hz, 1H), 8.00–7.91 (m, 2H), 7.89–7.82 (m, 2H), 7.57 (dtt, J = 8.4, 5.2, 2.3 Hz, 4H), 7.53–7.46 (m, 2H), 7.30 (dd, J = 6.8, 1.8 Hz, 2H), 7.05 (d, J = 14.9 Hz, 1H), 1.35 (s, 9H); ^{13}C NMR (100 MHz, $CDCl_3$): δ 188.5, 174.2, 161.9, 157.9, 157.8, 157.8, 157.5, 150.1, 147.2, 136.2, 134.7, 134.4, 134.3, 131.6, 130.1, 129.7, 128.7, 128.5, 127.9, 127.7, 127.2, 125.7, 121.5, 35.2, 31.0; HRMS m/z for $C_{27}H_{25}N_2O_2$ $[M + H]^+$. Calcd 409.1910, found 409.1909.

(*E*)-2-(3-(3-Methoxyphenyl)-3-oxoprop-1-en-1-yl)-3-phenylquinazolin-4(3*H*)-one (BE4136; 14). Yield: 196.5 mg (90%), yellow solid; m.p. = 203.4–204.8 °C; ^{1}H NMR (400 MHz, $CDCl_3$): δ 8.34 (dt, J = 7.8, 1.1 Hz, 1H), 8.21 (d, J = 14.9 Hz, 1H), 7.88–7.80 (m, 2H), 7.63–7.53 (m, 5H), 7.51 (dd, J = 2.7, 1.6 Hz, 1H), 7.40 (t, J = 7.9 Hz, 1H), 7.34–7.27 (m, 2H), 7.15 (ddd, J = 8.3, 2.7, 0.9 Hz, 1H), 7.05 (d, J = 14.9 Hz, 1H), 3.86 (s, 3H); ^{13}C NMR (100 MHz, $CDCl_3$): δ 188.8, 160.0, 150.0, 147.3, 138.3, 136.2, 134.8, 134.7, 131.5, 130.1, 129.7, 128.5, 128.0, 127.8, 127.3, 121.5, 120.1, 112.9, 55.5; HRMS m/z for $C_{24}H_{19}N_2O_3$ $[M + H]^+$. Calcd 383.1390, found 383.1389.

(*E*)-2-(3-(4-Methoxyphenyl)-3-oxoprop-1-en-1-yl)-3-phenylquinazolin-4(3*H*)-one (BE4133; 15). Yield: 145.9 mg (82%), yellow solid; m.p. = 228.7–230.1 °C; ^{1}H NMR (400 MHz, $CDCl_3$): δ 8.33 (d, J = 7.7 Hz, 1H), 8.25 (d, J = 14.9 Hz, 1H), 8.06–7.98 (m, 2H), 7.88–7.80 (m, 2H), 7.56 (tq, J = 8.4, 2.7 Hz, 4H), 7.34–7.27 (m, 2H), 7.04 (d, J = 14.9 Hz, 1H), 7.00–6.92 (m, 2H), 3.89 (s, 3H); ^{13}C NMR (100 MHz, $CDCl_3$): δ 187.1, 174.2, 164.0, 161.9, 150.2, 147.2, 136.2, 134.7, 133.9, 131.5, 131.2, 130.1, 130.0, 129.7, 128.5, 127.9, 127.7, 127.2, 121.5, 113.9, 55.5; HRMS m/z for $C_{24}H_{19}N_2O_3$ $[M + Na]^+$. Calcd 383.1390, found 383.1389.

(*E*)-2-(3-(2,4-Dimethoxyphenyl)-3-oxoprop-1-en-1-yl)-3-phenylquinazolin-4(3*H*)-one (BE4134; 16). Yield: 113.1 mg (70%), yellow solid; m.p. = 197.2–198.5 °C; ^{1}H NMR (400 MHz, $CDCl_3$): δ 8.36–8.29 (m, 1H), 8.27–8.17 (m, 1H), 7.81 (dd, J = 4.3, 1.7 Hz, 2H), 7.74 (d, J = 8.7 Hz, 1H), 7.62–7.48 (m, 4H), 7.33–7.24 (m, 3H), 6.92 (d, J = 14.9 Hz, 1H), 6.53 (dd, J = 8.7, 2.3 Hz, 1H), 6.47 (d, J = 2.2 Hz, 1H), 3.94 (s, 3H), 3.87 (s, 3H); ^{13}C NMR (100 MHz, $CDCl_3$): δ 188.4, 165.0, 162.0, 161.1, 150.7, 147.4, 136.7, 136.3, 134.6, 133.3, 131.7, 130.0, 129.6, 128.5, 127.9, 127.4, 127.2, 121.4, 121.0, 105.5, 98.4, 55.8, 55.6; LC-MS m/z = 413.52 $[M + H]^+$ for $C_{25}H_{21}N_2O_4$.

(*E*)-2-(3-(2-Fluoro-4-methoxyphenyl)-3-oxoprop-1-en-1-yl)-3-phenylquinazolin-4(3*H*)-one (BE4132; 17). Yield: 140.9 mg (80%), yellow solid; m.p. = 188.8–191.5 °C; ^{1}H NMR (400 MHz, $CDCl_3$): δ 8.33 (d, J = 7.9 Hz, 1H), 8.12 (dd, J = 14.9, 3.2 Hz, 1H), 7.87–7.77 (m, 3H), 7.62–7.48 (m, 4H), 7.35–7.27 (m, 2H), 7.01 (dd, J = 14.9, 1.6 Hz, 1H), 6.76 (dd, J = 8.9, 2.4 Hz, 1H), 6.64 (dd, J = 13.1, 2.4 Hz, 1H), 3.87 (s, 3H); ^{13}C NMR (100 MHz, $CDCl_3$): δ 185.7, 174.2, 165.3, 165.2, 161.9, 157.8, 150.1, 147.3, 136.2, 134.8, 134.7, 133.8, 132.7 (d, $J_{C,F}$ = 5.0 Hz), 130.1, 129.6, 128.5, 128.0, 127.7, 127.2, 121.5, 111.0 (d, $J_{C,F}$ = 3.0 Hz), 101.8 (d, $J_{C,F}$ = 27.0 Hz), 55.9; HRMS m/z for $C_{24}H_{18}FN_2O_3$ $[M + H]^+$. Calcd 401.1295, found 401.1295.

(*E*)-2-(3-Oxo-3-(2-(trifluoromethoxy)phenyl)prop-1-en-1-yl)-3-phenylquinazolin-4(3*H*)-one (BE4172; 18). Yield: 160.0 mg (66%), yellow solid; m.p. = >250 °C; ^{1}H NMR (400 MHz, $CDCl_3$): δ 8.33 (dt, J = 7.9, 1.1 Hz, 1H), 8.06 (dd, J = 15.0, 3.2 Hz, 1H), 7.87–7.79 (m, 2H), 7.74 (td, J = 7.6, 1.9 Hz, 1H), 7.63–7.49 (m, 5H), 7.33–7.27 (m, 2H), 7.23 (td, J = 7.5, 1.1 Hz, 1H), 7.15 (ddd, J = 11.0, 8.4, 1.1 Hz, 1H), 6.99 (dd, J = 15.0, 1.4

Hz, 1H); ^{13}C NMR (100 MHz, $CDCl_3$): δ 187.7 (d, $J_{C,F}$ = 3.0 Hz), 174.2, 162.8, 161.8, 160.3, 149.8, 147.2, 136.1, 134.9, 134.8, 134.7, 134.5, 134.5, 134.4, 130.9, 130.9, 130.1, 129.7, 128.5, 128.1, 127.8, 127.2, 126.0, 125.9, 124.5 (q, $J_{C,F}$ = 4.0 Hz), 121.5, 116.6 (d, $J_{C,F}$ = 20.0 Hz). HRMS *m*/*z* for $C_{24}H_{16}F_3N_2O_3$ $[M + H]^+$. Calcd 437.1107, found 437.1106.

(*E*)-2-(3-Oxo-3-(4-(trifluoromethoxy)phenyl)prop-1-en-1-yl)-3-phenylquinazolin-4(3*H*)-one (BE4175; 19). Yield: 193.7 mg (82%), yellow solid; m.p. = >250 °C; ^{1}H NMR (400 MHz, $CDCl_3$): δ 8.43 (dq, *J* = 8.0, 1.1 Hz, 1H), 8.31 (dd, *J* = 15.0, 0.8 Hz, 1H), 8.14 (ddt, *J* = 8.2, 5.1, 1.8 Hz, 2H), 7.94 (d, *J* = 4.0 Hz, 2H), 7.73–7.61 (m, 4H), 7.43–7.37 (m, 2H), 7.32–7.22 (m, 2H), 7.15 (dd, *J* = 14.9, 0.9 Hz, 1H); ^{13}C NMR (100 MHz, $CDCl_3$): δ 187.3, 167.2, 164.7, 161.8, 149.8, 147.1, 136.1, 134.9, 134.8, 133.3 (d, $J_{C,F}$ = 3.0 Hz), 131.5, 131.4, 130.9, 130.1, 129.7, 128.4, 127.9 (q, $J_{C,F}$ = 4.0 Hz), 127.3, 121.5, 115.9 (d, $J_{C,F}$ = 10.0 Hz); HRMS *m*/*z* for $C_{24}H_{16}F_3N_2O_3$ $[M + H]^+$. Calcd 437.1107, found 437.1106.

(*E*)-2-(3-(2-Fluorophenyl)-3-oxoprop-1-en-1-yl)-3-phenylquinazolin-4(3*H*)-one (BE4135; 20). Yield: 175.8 mg (85%), yellow solid; m.p. = 210.6–211.8 °C; ^{1}H NMR (400 MHz, $CDCl_3$): δ 8.33 (dt, *J* = 7.9, 1.1 Hz, 1H), 8.06 (dd, *J* = 15.0, 3.2 Hz, 1H), 7.87–7.79 (m, 2H), 7.74 (td, *J* = 7.6, 1.9 Hz, 1H), 7.63–7.49 (m, 5H), 7.32–7.27 (m, 2H), 7.23 (td, *J* = 7.5, 1.1 Hz, 1H), 7.15 (ddd, *J* = 11.0, 8.4, 1.1 Hz, 1H), 6.99 (dd, *J* = 15.0, 1.4 Hz, 1H); ^{13}C NMR (100 MHz, $CDCl_3$): δ 187.7 (d, $J_{C,F}$ = 3.0 Hz), 174.2, 162.8, 161.9, 160.3, 149.8, 147.2, 136.1, 134.9, 134.8, 134.7, 134.5, 134.5, 134.4, 130.9 (d, $J_{C,F}$ = 2.0 Hz), 130.1, 129.7, 128.5, 128.1, 127.8, 127.2, 126.0, 125.9, 124.6 (d, $J_{C,F}$ = 4.0 Hz), 121.5, 116.6 (d, $J_{C,F}$ = 22.0 Hz); HRMS *m*/*z* for $C_{23}H_{16}FN_2O_2$ $[M + H]^+$. Calcd 371.1190, found 371.1189.

(*E*)-2-(3-(4-Fluorophenyl)-3-oxoprop-1-en-1-yl)-3-phenylquinazolin-4(3*H*)-one (BE4118; 21). Yield: 107.2 mg (90%), yellow solid; m.p. = 223.4–224.9 °C; ^{1}H NMR (400 MHz, $CDCl_3$): δ 8.34 (dq, *J* = 8.0, 1.1 Hz, 1H), 8.21 (dd, *J* = 15.0, 0.8 Hz, 1H), 8.04 (ddt, *J* = 8.2, 5.1, 1.8 Hz, 2H), 7.84 (d, *J* = 4.0 Hz, 2H), 7.66–7.50 (m, 4H), 7.35–7.27 (m, 2H), 7.22–7.12 (m, 2H), 7.06 (dd, *J* = 14.9, 0.9 Hz, 1H); ^{13}C NMR (100 MHz, $CDCl_3$): δ 187.3, 167.3, 164.7, 161.8, 149.8, 147.1, 136.1, 134.9, 134.8, 133.3 (d, $J_{C,F}$ = 3.0 Hz), 131.4 (d, $J_{C,F}$ = 10.0 Hz), 130.9, 130.1, 129.7, 128.5, 127.9 (d, $J_{C,F}$ = 3.0 Hz), 127.3, 121.55, 115.9 (d, $J_{C,F}$ = 20.0 Hz); HRMS *m*/*z* for $C_{23}H_{16}FN_2O_2$ $[M + H]^+$. Calcd 371.1190, found 371.1189.

(*E*)-2-(3-(2-Chlorophenyl)-3-oxoprop-1-en-1-yl)-3-phenylquinazolin-4(3*H*)-one (BE4164; 22). Yield: 120.0 mg (73%), yellow solid; m.p. = 182.6–185.1 °C; ^{1}H NMR (400 MHz, $CDCl_3$): δ 8.23 (d, *J* = 7.9 Hz, 1H), 7.79–7.65 (m, 3H), 7.53–7.37 (m, 4H), 7.33–7.22 (m, 3H), 7.18 (ddt, *J* = 7.7, 5.9, 2.1 Hz, 3H), 6.67 (dd, *J* = 15.3, 1.2 Hz, 1H); ^{13}C NMR (100 MHz, $CDCl_3$): δ 192.1, 161.7, 149.6, 147.1, 137.8, 136.0, 135.5, 134.8, 134.6, 132.0, 131.5, 130.3, 130.0, 129.6, 129.5, 128.4, 128.1, 127.9, 127.2, 126.8, 121.5; HRMS *m*/*z* for $C_{23}H_{16}ClN_2O_2$ $[M + H]^+$. Calcd 387.0894, found 387.0893.

(*E*)-2-(3-(4-Chlorophenyl)-3-oxoprop-1-en-1-yl)-3-phenylquinazolin-4(3*H*)-one (BE4122; 23). Yield: 130.2 mg (90%), yellow solid; m.p. = 226.4–227.8 °C; ^{1}H NMR (400 MHz, $CDCl_3$): δ 8.34 (dt, *J* = 7.9, 1.1 Hz, 1H), 8.19 (d, *J* = 14.9 Hz, 1H), 7.99–7.90 (m, 2H), 7.89–7.80 (m, 2H), 7.64–7.52 (m, 4H), 7.51–7.42 (m, 2H), 7.33–7.27 (m, 2H), 7.06 (d, *J* = 14.9 Hz, 1H); ^{13}C NMR (100 MHz, $CDCl_3$): δ 187.7, 161.8, 149.8, 147.2, 140.1, 136.1, 135.3, 135.1, 134.8, 130.8, 130.1, 129.8, 129.1, 128.5, 127.9, 127.9, 127.3, 121.6; HRMS *m*/*z* for $C_{23}H_{16}ClN_2O_2$ $[M + H]^+$. Calcd 387.0894, found 387.0893.

(*E*)-2-(3-(2,5-Dichlorophenyl)-3-oxoprop-1-en-1-yl)-3-phenylquinazolin-4(3*H*)-one (BE4130; 24). Yield: 171.0 mg (80%), yellow solid; m.p. = 202.6–204.5 °C; ^{1}H NMR (400 MHz, $CDCl_3$): δ 8.31 (dd, *J* = 8.1, 1.3 Hz, 1H), 8.06 (d, *J* = 14.8 Hz, 1H), 7.88 (dd, *J* = 3.9, 1.1 Hz, 1H), 7.85–7.79 (m, 2H), 7.70 (dd, *J* = 4.9, 1.1 Hz, 1H), 7.54 (dqt, *J* = 7.1, 5.3, 2.3 Hz, 4H), 7.27 (dd, *J* = 8.0, 1.7 Hz, 2H), 7.16 (t, *J* = 4.3 Hz, 1H), 7.05 (d, *J* = 14.8 Hz, 1H); ^{13}C NMR (100 MHz, $CDCl_3$): δ 186.7, 161.8 149.6, 147.1, 138.2, 136.5, 136.0, 135.7, 134.8, 133.5, 130.9, 130.6, 130.2, 130.0, 129.8, 128.6, 128.4, 128.0, 128.0, 127.7, 127.3, 121.6; HRMS *m*/*z* for $C_{23}H_{15}Cl_2N_2O_2$ $[M + H]^+$. Calcd 421.0505, found 421.0503.

(*E*)-2-(3-(3,4-Dichlorophenyl)-3-oxoprop-1-en-1-yl)-3-phenylquinazolin-4(3*H*)-one (BE4173, 25). Yield: 230.0 mg (86%), yellow solid; m.p. = 210.4–212.2 °C; ^{1}H NMR (400 MHz, $CDCl_3$): δ 8.42 (d, *J* = 7.9 Hz, 1H), 8.21 (d, *J* = 14.9 Hz, 1H), 8.14 (d, *J* = 2.0 Hz, 1H), 7.98–7.87 (m, 3H), 7.66 (dq, *J* = 8.1, 5.2 Hz, 6H), 7.42–7.35 (m, 2H), 7.15 (d, *J* = 14.9 Hz, 1H); ^{13}C NMR (100 MHz, $CDCl_3$): δ 186.7, 174.2, 161.8, 149.6, 147.1, 138.2, 136.5, 136.0, 135.7, 134.8, 133.5, 130.9, 130.6, 130.2, 130.0, 129.8, 128.4, 128.0, 128.0, 127.7, 127.3, 121.6; HRMS *m*/*z* for $C_{23}H_{15}Cl_2N_2O_2$ [M + H]+. Calcd 421.0505, found 421.0503.

(*E*)-2-(3-(4-Bromophenyl)-3-oxoprop-1-en-1-yl)-3-phenylquinazolin-4(3*H*)-one (BE4119; 26). Yield: 129.7 mg (90%), yellow solid; m.p. = 225.6–227.2 °C; ^{1}H NMR (400 MHz, $CDCl_3$): δ 8.34 (dd, *J* = 8.0, 1.4 Hz, 1H), 8.18 (dd, *J* = 15.0, 1.0 Hz, 1H), 7.92–7.79 (m, 4H), 7.69–7.50 (m, 6H), 7.36–7.27 (m, 2H), 7.06 (dd, *J* = 14.9, 1.1 Hz, 1H); ^{13}C NMR (100 MHz, $CDCl_3$): δ 187.9, 161.8, 149.8, 147.1, 136.1, 135.6, 135.2, 134.8, 132.1, 130.7, 130.2, 130.1, 129.8, 128.9, 128.5, 127.9, 127.3, 121.5; HRMS *m*/*z* for $C_{23}H_{16}BrN_2O_2$ $[M + H]^+$. Calcd 431.0389, found 431.0387.

(*E*)-2-(3-(4-Nitrophenyl)-3-oxoprop-1-en-1-yl)-3-phenylquinazolin-4(3*H*)-one (BE4170, 27). Yield: 160.0 mg (87%), brown solid; m.p. = 184.8–186.4 °C; ^{1}H NMR (400 MHz, $CDCl_3$): δ 8.28 (dd, *J* = 8.2, 5.5 Hz, 3H), 8.15 (d, *J* = 14.9 Hz, 1H), 8.08 (d, *J* = 8.6 Hz, 2H), 7.85–7.76 (m, 2H), 7.61–7.46 (m, 4H), 7.29–7.22 (m, 2H), 7.05 (d, *J* = 14.9 Hz, 1H); ^{13}C NMR (100 MHz, $CDCl_3$): δ 187.6, 174.2, 161.7, 150.4, 149.4, 147.0, 141.4, 136.4, 136.0, 134.9, 130.2, 130.2, 129.9, 129.7, 128.4, 128.2, 128.0, 127.3, 123.9, 121.6; HRMS *m*/*z* for $C_{23}H_{16}N_3O_4$ $[M + H]^+$. Calcd 398.1135, found 398.1133.

(*E*)-2-(3-(Naphthalen-2-yl)-3-oxoprop-1-en-1-yl)-3-phenylquinazolin-4(3*H*)-one (BE4160; 28). Yield: 109.0 mg (60%), yellow solid; m.p. = >250 °C; ^{1}H NMR (400 MHz, $CDCl_3$): δ 8.57 (s, 1H), 8.41 (d, *J* = 14.9 Hz, 1H), 8.36 (d, *J* = 7.9 Hz, 1H), 8.09–7.98 (m, 2H), 7.95–7.83 (m, 4H), 7.69–7.51 (m, 6H), 7.37–7.29 (m, 2H), 7.13 (d, *J* = 14.9 Hz, 1H); ^{13}C NMR (100 MHz, $CDCl_3$): δ 188.7, 161.9, 150.1, 147.2, 136.2, 135.8, 134.8, 134.6, 134.3,

132.4, 131.4, 130.8, 130.1, 129.8, 129.7, 128.9, 128.8, 128.5, 127.9, 127.8, 127.3, 126.9, 124.1, 121.6; HRMS *m*/*z* for $C_{27}H_{19}N_2O_2$ $[M + H]^+$. Calcd 403.1441, found 403.1439.

(*E*)-2-(3-(Benzo[*d*][1,3]dioxol-5-yl)-3-oxoprop-1-en-1-yl)-3-phenylquinazolin-4(3*H*)-one (BE4174; 29). Yield: 190.0 mg (75%), yellow solid; m.p. = 236.3–238.5 °C; ^{1}H NMR (400 MHz, $CDCl_3$): δ 8.33 (d, J = 7.9 Hz, 1H), 8.19 (d, J = 14.9 Hz, 1H), 7.84 (d, J = 3.9 Hz, 2H), 7.66 (dd, J = 8.2, 1.8 Hz, 1H), 7.57 (tdd, J = 10.9, 7.0, 3.3 Hz, 5H), 7.47 (d, J = 1.7 Hz, 1H), 7.34–7.27 (m, 2H), 7.03 (d, J = 14.9 Hz, 1H), 6.88 (d, J = 8.2 Hz, 1H), 6.06 (s, 2H); ^{13}C NMR (100 MHz, $CDCl_3$): δ 186.7, 174.2, 161.9, 152.4, 150.1, 148.4, 147.2, 136.2, 134.7, 134.5, 134.2, 131.9, 131.3, 130.1, 130.0, 129.7, 128.6, 128.4, 127.9, 127.8, 127.7, 127.2, 127.1, 125.5, 121.5, 108.3, 107.9, 102.0; HRMS *m*/*z* for $C_{24}H_{17}N_2O_4$ $[M + H]^+$. Calcd 397.1182, found 397.1181.

(*E*)-2-(3-Oxo-3-(thiophen-2-yl)prop-1-en-1-yl)-3-phenylquinazolin-4(3*H*)-one (BE4131; 30). Yield: 158.5 mg (85%), yellow solid; m.p. = >250 °C; ^{1}H NMR (400 MHz, $CDCl_3$): δ 8.34 (dt, J = 7.8, 1.1 Hz, 1H), 8.09 (d, J = 14.8 Hz, 1H), 7.90 (dd, J = 3.8, 1.1 Hz, 1H), 7.88–7.82 (m, 2H), 7.72 (dd, J = 4.9, 1.1 Hz, 1H), 7.63–7.51 (m, 4H), 7.33–7.27 (m, 2H), 7.19 (dd, J = 4.9, 3.8 Hz, 1H), 7.08 (d, J = 14.8 Hz, 1H); ^{13}C NMR (100 MHz, $CDCl_3$): δ 180.8, 161.8, 149.8, 147.2, 144.7, 136.1, 135.3, 134.8, 134.1, 133.1, 131.2, 130.1, 130.0, 129.7, 128.4, 127.9, 127.8, 127.2, 121.5; HRMS *m*/*z* for $C_{21}H_{15}N_2O_2S$ $[M + H]^+$. Calcd 359.0848, found 359.0847.

(*E*)-2-(3-([1,1′-Biphenyl]-4-yl)-3-oxoprop-1-en-1-yl)-3-phenylquinazolin-4(3*H*)-one (BE4171, 31). Yield: 220.0 mg (81%), yellow solid; m.p. = 217.2–219.7 °C; ^{1}H NMR (400 MHz, $CDCl_3$): δ 8.38–8.33 (m, 1H), 8.29 (d, J = 14.9 Hz, 1H), 8.09 (d, J = 8.3 Hz, 2H), 7.90–7.82 (m, 2H), 7.72 (d, J = 8.3 Hz, 2H), 7.68–7.53 (m, 7H), 7.49 (t, J = 7.3 Hz, 2H), 7.46–7.39 (m, 1H), 7.35–7.29 (m, 2H), 7.09 (d, J = 14.9 Hz, 1H); ^{13}C NMR (100 MHz, $CDCl_3$): δ 188.4, 174.2, 161.9, 158.0, 150.0, 147.2, 146.3, 139.6, 136.2, 135.6, 134.8, 134.6, 131.4, 130.1, 130.0, 129.7, 129.4, 128.9, 128.6, 128.5, 128.4, 127.9, 127.8, 127.4, 127.3, 127.3, 121.5; HRMS *m*/*z* for $C_{29}H_{21}N_2O_2$ $[M + H]^+$. Calcd 429.1575, found 429.1596.

(*E*)-3-(4-Fluorophenyl)-2-(3-oxo-3-phenylprop-1-en-1-yl)quinazolin-4(3*H*)-one (BE4123; 32). Yield: 143.4 mg (92%), yellow solid; m.p. = 228.7–230.2 °C; ^{1}H NMR (400 MHz, $CDCl_3$): δ 8.33 (dt, J = 8.0, 1.1 Hz, 1H), 8.27 (d, J = 14.9 Hz, 1H), 8.07–7.99 (m, 2H), 7.89–7.81 (m, 2H), 7.65–7.59 (m, 1H), 7.56 (dt, J = 8.2, 4.2 Hz, 1H), 7.51 (t, J = 7.6 Hz, 2H), 7.32–7.24 (m, 4H), 7.06 (d, J = 14.9 Hz, 1H); ^{13}C NMR (100 MHz, $CDCl_3$): δ 187.7, 161.8, 149.8, 147.2, 140.1, 136.1, 135.3, 135.1, 134.8, 130.8, 130.1, 129.8, 129.1, 128.5, 127.9 (d, $J_{C,F}$ = 4.0 Hz), 127.3, 121.6; HRMS *m*/*z* for $C_{23}H_{16}FN_2O_2$ $[M + H]^+$. Calcd 371.1190, found 371.1190.

(*E*)-2-(3-(4-Chlorophenyl)-3-oxoprop-1-en-1-yl)-3-(4-fluorophenyl)quinazolin-4(3*H*)-one (BE4125; 33). Yield: 147.3 mg (89%), pale yellow solid; m.p. = 205.2–206.4 °C; ^{1}H NMR (400 MHz, $CDCl_3$): δ 8.34 (d, J = 7.9 Hz, 1H), 8.19 (d, J = 14.9 Hz, 1H), 7.98–7.91 (m, 2H), 7.89–7.81 (m, 2H), 7.65–7.51 (m, 5H), 7.50–7.42 (m, 2H), 7.29 (ddd, J = 7.0, 3.7, 1.6 Hz, 3H), 7.06 (d, J = 14.9 Hz, 1H); ^{13}C NMR (100 MHz, $CDCl_3$): δ 187.7, 161.9 (d, $J_{C,F}$ = 8.0 Hz), 149.9 (d, $J_{C,F}$ = 12.0 Hz), 147.1, 140.1, 136.1, 135.1, 134.8, 130.7, 130.1, 129.8, 129.1, 128.5, 127.9, 127.3, 121.5; HRMS *m*/*z* for $C_{23}H_{15}ClFN_2O_2$ $[M + H]^+$. Calcd 405.0800, found 405.0799.

(*E*)-2-(3-(4-Bromophenyl)-3-oxoprop-1-en-1-yl)-3-(4-fluorophenyl)quinazolin-4(3*H*)-one (BE4128; 34). Yield: 174.9 mg (90%), yellow solid; m.p. = 210.9–212.8 °C; ^{1}H NMR (400 MHz, $CDCl_3$): δ 8.32 (dt, J = 8.0, 1.1 Hz, 1H), 8.20 (d, J = 14.8 Hz, 1H), 7.94–7.86 (m, 2H), 7.86–7.80 (m, 2H), 7.69–7.61 (m, 2H), 7.56 (ddd, J = 8.2, 5.1, 3.2 Hz, 1H), 7.27 (d, J = 6.2 Hz, 4H), 7.06 (d, J = 14.8 Hz, 1H); ^{13}C NMR (100 MHz, $CDCl_3$): δ 187.7, 164.2, 161.8 (d, $J_{C,F}$ = 17.0 Hz), 149.6, 147.0, 135.6, 134.9 (d, $J_{C,F}$ = 14.0 Hz), 132.1, 131.9 (d, $J_{C,F}$ = 3.0 Hz), 130.8, 130.3 (d, $J_{C,F}$ = 9.0 Hz), 130.2, 129.0, 128.0 (d, $J_{C,F}$ = 6.0 Hz), 127.3, 121.4, 117.2 (d, $J_{C,F}$ = 23.0 Hz); HRMS *m*/*z* for $C_{23}H_{15}BrFN_2O_2$ $[M + H]^+$. Calcd 449.0295, found 449.0293.

(*E*)-3-(4-Fluorophenyl)-2-(3-oxo-3-(*p*-tolyl)prop-1-en-1-yl)quinazolin-4(3*H*)-one (BE4126; 35). Yield: 141.5 mg (90%), pale yellow solid; m.p. = 232.6–234.5 °C; ^{1}H NMR (400 MHz, $CDCl_3$): δ 8.35 (dt, J = 8.0, 1.1 Hz, 1H), 8.27 (d, J = 14.9 Hz, 1H), 8.00–7.92 (m, 2H), 7.90–7.84 (m, 2H), 7.58 (ddd, J = 8.2, 4.8, 3.6 Hz, 1H), 7.37–7.24 (m, 8H), 7.07 (d, J = 14.9 Hz, 1H), 2.46 (s, 3H); ^{13}C NMR (100 MHz, $CDCl_3$): δ 188.3, 161.9, 150.0, 147.2, 144.7, 134.9, 134.4, 134.0, 131.8, 130.4 (d, $J_{C,F}$ = 9.0 Hz), 129.5, 128.9, 127.9 (d, $J_{C,F}$ = 11.0 Hz), 127.3, 121.43, 117.2 (d, $J_{C,F}$ = 23.0 Hz), 21.7; HRMS *m*/*z* for $C_{24}H_{18}FN_2O_2$ $[M + H]^+$. Calcd 385.1346, found 385.1345.

(*E*)-2-(3-(4-Ethylphenyl)-3-oxoprop-1-en-1-yl)-3-(4-fluorophenyl)quinazolin-4(3*H*)-one (BE4127; 36). Yield: 139.8 mg (85%), yellow sold; m.p. = 229.6–231.2 °C; ^{1}H NMR (400 MHz, $CDCl_3$): δ 8.36–8.30 (m, 1H), 8.26 (d, J = 14.9 Hz, 1H), 7.99–7.92 (m, 2H), 7.88–7.83 (m, 2H), 7.61–7.52 (m, 1H), 7.33 (d, J = 8.1 Hz, 2H), 7.30–7.23 (m, 6H), 7.05 (d, J = 14.9 Hz, 1H), 2.73 (q, J = 7.6 Hz, 2H), 1.28 (t, J = 7.7 Hz, 3H); ^{13}C NMR (100 MHz, $CDCl_3$): δ 188.4, 150.9, 147.2, 134.9, 134.7, 134.0, 131.8, 130.4 (d, $J_{C,F}$ = 9.0 Hz), 129.1, 128.3, 127.9 (d, $J_{C,F}$ = 11.0 Hz), 127.3, 121.4, 117.2 (d, $J_{C,F}$ = 14.0 Hz), 29.0, 15.1; HRMS *m*/*z* for $C_{25}H_{20}FN_2O_2$ $[M + H]^+$. Calcd 399.1503, found 399.1501.

(*E*)-2-(3-(4-(*tert*-Butyl)phenyl)-3-oxoprop-1-en-1-yl)-3-(4-fluorophenyl)quinazolin-4(3*H*)-one (BE4176, 37). Yield: 301.92 mg (90%), yellow solid; m.p. = 223.3–225.6 °C; ^{1}H NMR (400 MHz, $CDCl_3$): δ 8.30 (d, J = 8.0 Hz, 1H), 8.23 (d, J = 14.9 Hz, 1H), 7.98–7.90 (m, 2H), 7.82 (d, J = 4.0 Hz, 2H), 7.58–7.43 (m, 3H), 7.32–7.19 (m, 5H), 7.02 (dd, J = 14.8, 1.7 Hz, 1H), 1.33 (s, 9H); ^{13}C NMR (100 MHz, $CDCl_3$): δ 188.4, 164.1, 161.8 (d, $J_{C,F}$ = 29.0 Hz), 157.6, 149.9, 147.2, 134.9, 134.3, 134.0, 131.8, 130.4, 130.3, 128.8, 128.0, 127.9, 127.7, 127.2, 125.7, 121.4, 117.2 (d, $J_{C,F}$ = 23.0 Hz), 35.2, 31.0; HRMS *m*/*z* for $C_{27}H_{24}FN_2O_2$ $[M + H]^+$. Calcd 427.1816, found 427.1814.

(*E*)-6-Fluoro-2-(3-oxo-3-phenylprop-1-en-1-yl)-3-phenylquinazolin-4(3*H*)-one (BE4166; 38). Yield: 161.0 mg (73%), yellow solid; m.p. = 228.2–230.4 °C; ^{1}H NMR (400 MHz, $CDCl_3$): δ 8.21 (d, J = 15.0 Hz, 1H), 8.03–7.93 (m, 3H), 7.89–7.82 (m, 1H), 7.65–7.52 (m, 5H), 7.49 (dd, J = 8.4, 7.1 Hz, 2H), 7.29 (dt, J = 7.7, 1.4 Hz, 2H), 7.04 (d, J = 14.9 Hz, 1H); ^{13}C NMR (100 MHz, $CDCl_3$): δ 188.9, 162.7, 161.2 (d, $J_{C,F}$ = 4.0 Hz), 160.2, 149.3,

143.9 (d, $J_{C,F}$ = 2.0 Hz), 136.9, 135.9, 134.4, 133.6, 131.4, 130.4 (d, $J_{C,F}$ = 9.0 Hz), 130.2, 129.87, 128.7 (d, $J_{C,F}$ = 3.0 Hz), 128.5, 128.4, 123.4 (d, $J_{C,F}$ = 24.0 Hz), 122.9 (d, $J_{C,F}$ = 9.0 Hz), 112.2 (d, $J_{C,F}$ = 24.0 Hz); HRMS *m*/*z* for $C_{23}H_{16}FN_2O_2$ $[M + H]^+$. Calcd 371.1190, found 371.1189.

(*E*)-2-(3-(4-(*tert*-Butyl)phenyl)-3-oxoprop-1-en-1-yl)-6-fluoro-3-phenylquinazolin-4(3*H*)-one (BE4167; 39). Yield: 210.0 mg (83%), pale yellow solid; m.p. = 212.4–214.2 °C; ^{1}H NMR (400 MHz, $CDCl_3$): δ 8.22 (dd, J = 15.0, 1.0 Hz, 1H), 7.95 (dd, J = 8.4, 6.3 Hz, 3H), 7.86 (dd, J = 9.0, 4.9 Hz, 1H), 7.64–7.53 (m, 4H), 7.50 (d, J = 8.5 Hz, 2H), 7.34–7.27 (m, 2H), 7.03 (dd, J = 14.9, 1.1 Hz, 1H), 1.35 (s, 9H); ^{13}C NMR (100 MHz, $CDCl_3$): δ 188.4, 174.1, 174.1, 174.1, 174.1, 161.2 (d, $J_{C,F}$ = 2.0 Hz), 157.5, 149.5, 143.9 (d, $J_{C,F}$ = 2.0 Hz), 136.0, 134.3, 134.0, 131.6, 130.4 (d, $J_{C,F}$ = 9.0 Hz), 130.2, 129.8, 128.7, 128.4, 125.7, 123.4 (d, $J_{C,F}$ = 24.0 Hz), 122.9 (d, $J_{C,F}$ = 8.0 Hz), 112.2 (d, $J_{C,F}$ = 23.0 Hz), 35.2, 31.0; HRMS *m*/*z* for $C_{27}H_{24}FN_2O_2$ $[M + H]^+$. Calcd 427.1816, found 427.1815.

(*E*)-2-(3-Oxo-3-phenylprop-1-en-1-yl)-3-phenyl-7-(trifluoromethyl)quinazolin-4(3*H*)-one (BE4165; 40). Yield: 155.4 mg (75%), yellow solid; m.p. = 212.6–214.9 °C; ^{1}H NMR (400 MHz, $CDCl_3$): δ 8.45 (d, J = 8.3 Hz, 1H), 8.30 (d, J = 14.9 Hz, 1H), 8.14 (s, 1H), 8.01 (dd, J = 8.3, 1.3 Hz, 2H), 7.75 (dd, J = 8.3, 1.7 Hz, 1H), 7.60 (dtd, J = 11.2, 7.2, 5.5 Hz, 5H), 7.51 (t, J = 7.6 Hz, 2H), 7.34–7.28 (m, 2H), 7.05 (d, J = 14.9 Hz, 1H); ^{13}C NMR (100 MHz, $CDCl_3$): δ 188.7, 174.1, 161.1, 157.1, 151.3, 147.2, 136.8, 135.7, 134.0, 133.7, 132.3, 130.3, 130.0, 128.8, 128.8, 128.4, 128.3, 125.5 (d, $J_{C,F}$ = 4.0 Hz), 123.8, 122.0; HRMS *m*/*z* for $C_{24}H_{16}F_3N_2O_2$ $[M + H]^+$. Calcd 421.1158, found 421.1157.

(*E*)-2-(3-(4-(*tert*-Butyl)phenyl)-3-oxoprop-1-en-1-yl)-3-phenyl-7-(trifluoromethyl)quinazolin-4(3*H*)-one (BE4168; 41). Yield: 190.0 mg (81%), pale yellow solid; m.p. = 180.4–2182.6 °C; ^{1}H NMR (400 MHz, $CDCl_3$): δ 8.44 (d, J = 8.3 Hz, 1H), 8.30 (d, J = 14.9 Hz, 1H), 8.14 (s, 1H), 8.00–7.91 (m, 2H), 7.74 (dd, J = 8.3, 1.7 Hz, 1H), 7.65–7.54 (m, 3H), 7.52 (d, J = 8.4 Hz, 2H), 7.34–7.27 (m, 2H), 7.03 (d, J = 14.9 Hz, 1H), 1.36 (s, 9H); ^{13}C NMR (100 MHz, $CDCl_3$): δ 188.3, 178.9, 174.2(q, $J_{C,F}$ = 5.0 Hz), 157.8 (d, $J_{C,F}$ = 15.0 Hz), 151.4, 134.3, 133.6, 132.5, 130.3, 130.0, 128.8, 128.4, 128.3 (q, $J_{C,F}$ = 2.0 Hz), 125.8, 123.6, 109.9, 35.2, 31.0; HRMS *m*/*z* for $C_{28}H_{24}F_3N_2O_2$ $[M + H]^+$. Calcd 477.1784, found 477.1783.

(*E*)-2-(3-(3,4-Dimethoxyphenyl)-3-oxoprop-1-en-1-yl)-3-phenyl-7-(trifluoromethyl)quinazolin-4(3*H*)-one (BE4163; 42). Yield: 177.6 mg (75%), yellow solid; m.p. = 213.8–215.6 °C; ^{1}H NMR (400 MHz, $CDCl_3$): δ 8.44 (d, J = 8.3 Hz, 1H), 8.30 (d, J = 14.8 Hz, 1H), 8.19–8.11 (m, 1H), 7.73 (td, J = 8.1, 1.9 Hz, 2H), 7.64–7.52 (m, 4H), 7.34–7.27 (m, 2H), 7.03 (d, J = 14.8 Hz, 1H), 6.93 (d, J = 8.4 Hz, 1H), 3.98 (s, 3H), 3.94 (s, 3H); ^{13}C NMR (100 MHz, $CDCl_3$): δ 186.8, 161.2, 154.1, 151.5, 149.4, 147.3, 136.5, 136.1, 135.7, 133.3, 132.1, 130.2, 130.1, 130.0, 128.4, 128.3, 125.4 (d, $J_{C,F}$ = 4.0 Hz), 123.9, 123.8, 123.5 (q, $J_{C,F}$ = 4.0 Hz), 110.2 (d, $J_{C,F}$ = 48.0 Hz), 56.1, 56.0; HRMS *m*/*z* for $C_{26}H_{20}F_3N_2O_4$ $[M + H]^+$. Calcd 481.1369, found 481.1368.

(*E*)-2-(3-([1,1′-Biphenyl]-4-yl)-3-oxoprop-1-en-1-yl)-3-phenyl-7-(trifluoromethyl)quinazolin-4(3*H*)-one (BE4177; 43). Yield: 198.2 mg (81%), yellow solid; m.p. = 242.8–244.3 °C; ^{1}H NMR (400 MHz, $CDCl_3$): δ 8.45 (d, J = 8.3 Hz, 1H), 8.35 (dd, J = 14.9, 1.2 Hz, 1H), 8.16 (s, 1H), 8.14–8.06 (m, 2H), 7.78–7.70 (m, 3H), 7.71–7.56 (m, 6H), 7.54–7.46 (m, 2H), 7.46–7.39 (m, 1H), 7.32 (dt, J = 7.8, 1.4 Hz, 2H), 7.25 (d, J = 7.5 Hz, 1H), 7.18 (d, J = 7.6 Hz, 1H), 7.08 (dd, J = 14.9, 1.2 Hz, 1H); ^{13}C NMR (100 MHz, $CDCl_3$): δ 188.1, 173.8 (d, $J_{C,F}$ = 3.0 Hz), 161.1, 151.4, 147.3, 146.4, 139.6, 136.2, 135.7, 135.5, 133.9, 132.2, 130.3, 130.0, 129.4, 129.0, 128.4, 128.3, 128.2, 127.4, 127.3, 125.5 (d, $J_{C,F}$ = 4.0 Hz), 125.3, 123.8, 123.6 (d, $J_{C,F}$ = 3.0 Hz); HRMS *m*/*z* for $C_{30}H_{20}F_3N_2O_2$ $[M + H]^+$. Calcd 497.1471, found 497.1470.

TLX ligand screening assay

A biochemical assay was used to characterize ligand binding to TLX by detecting alteration in the ability of the TLX ligand binding domain to recruit an NR box peptide derived from the nuclear receptor-interacting protein 1 (NR1P1; receptor-interacting protein 140 (RIP140) transcriptional cofactor). RIP140 has been previously identified as a TLX interacting protein.[61] AlphaScreen (Revvity) technology was used to detect the TLX-RIP140 NR box peptide interaction. Detailed protocol is described in Markham *et al.*, 2024.[59]

Molecular modeling

Modeling of selected ligands were manually derived from BMS493, with their chalcone moieties overlapping with the phenyl ethynyl group of BMS493 while keeping their quinazolinone moieties near the proximity of the fused aromatic rings of BMS493 in the most probable conformation of the TLX-BMS493 complex extracted from a 1 μs molecular dynamics (MD) simulation performed previously.[55] Receptor conformations were obtained from induced-fit docking of these ligands using the Maestro software suite.[62] Energy minimization, comprising 100 steepest descent steps followed by 10 conjugate gradient steps, was executed with the AMBER FF14SB force field[63] in UCSF Chimera.[64]

Conflicts of interest

There are no conflicts to declare.

Data availability

The datasets supporting this article, including synthetic procedures, spectroscopic characterization, and computational models, are available within the main text and ESI.† Additional raw data or experimental details are available from the corresponding author upon reasonable request.

Acknowledgements

This work was financially supported by the Center for Clinical Pharmacology, Washington University School of Medicine, and the University of Health Sciences and Pharmacy in St Louis, St Louis, MO 63110.

References

1 P. S. Auti, G. George and A. T. Paul, *RSC Adv.*, 2020, **10**, 41353–41392.
2 U. A. Kshirsagar, *Org. Biomol. Chem.*, 2015, **13**, 9336–9352.
3 I. Khan, A. Ibrar, N. Abbas and A. Saeed, *Eur. J. Med. Chem.*, 2014, **76**, 193–244.
4 Q. Dherbassy, S. Manna, C. Shi, W. Prasitwatcharakorn, G. E. M. Crisenza, G. J. P. Perry and D. J. Procter, *Angew. Chem., Int. Ed.*, 2021, **60**, 14355–14359.
5 Y. Hao, K. Wang, Z. Wang, Y. Liu, D. Ma and Q. Wang, *J. Agric. Food Chem.*, 2020, **68**, 8764–8773.
6 S. B. Mhaske and N. P. Argade, *Tetrahedron*, 2006, **62**, 9787–9826.
7 I. Khan, S. Zaib, S. Batool, N. Abbas, Z. Ashraf, J. Iqbal and A. Saeed, *Bioorg. Med. Chem.*, 2016, **24**, 2361–2381.
8 M. H. Hekal and F. S. M. Abu El-Azm, *Synth. Commun.*, 2018, **48**, 2391–2402.
9 F. Hakim, R. Salfi, D. Bhikshapathi and A. Khan, *Anticancer Agents Med. Chem.*, 2022, **22**, 926–932.
10 A. L. Chen and K. K. Chen, *J. Am. Pharm. Assoc.*, 1933, **22**, 716–719.
11 J. Bergman and S. Bergman, *J. Org. Chem.*, 1985, **50**, 1246–1255.
12 T. C. Moon, M. Murakami, I. Kudo, K. H. Son, H. P. Kim, S. S. Kang and H. W. Chang, *Inflammation Res.*, 1999, **48**, 621–625.
13 T. Nomura, Z.-Z. Ma, Y. Hano and Y.-J. Chen, *Heterocycles*, 1997, **46**, 541.
14 H. Wang and A. Ganesan, *Tetrahedron Lett.*, 1998, **39**, 9097–9098.
15 Y. Rao, H. Liu, L. Gao, H. Yu, J.-H. Tan, T.-M. Ou, S.-L. Huang, L.-Q. Gu, J.-M. Ye and Z.-S. Huang, *Bioorg. Med. Chem.*, 2015, **23**, 4719–4727.
16 K. Zirlik and H. Veelken, Idelalisib. In *Small Molecules in Hematology*, ed. U. Martens, Springer, 2018, pp. 243–264.
17 T. D. Shanafelt, B. J. Borah, H. D. Finnes, K. G. Chaffee, W. Ding, J. F. Leis, A. A. Chanan-Khan, S. A. Parikh, S. L. Slager, N. E. Kay and T. G. Call, *J. Oncol. Pract.*, 2015, **11**, 252–258.
18 B. H. Rotstein, S. Zaretsky, V. Rai and A. K. Yudin, *Chem. Rev.*, 2014, **114**, 8323–8359.
19 J. Peng, T. Lin, W. Wang, Z. Xin, T. Zhu, Q. Gu and D. Li, *J. Nat. Prod.*, 2013, **76**, 1133–1140.
20 C. Du, Y. Zhang, T. Li, Z. Zha and Z. Wang, *Chem. Commun.*, 2024, **60**, 5274–5277.
21 K. Donthiboina, H. K. Namballa, S. P. Shaik, J. B. Nanubolu, N. Shankaraiah and A. Kamal, *Org. Biomol. Chem.*, 2018, **16**, 1720–1727.
22 M. Ashraf-Uz-Zaman, X. Li, Y. Yao, C. B. Mishra, B. K. Moku and Y. Song, *J. Med. Chem.*, 2023, **66**, 10746–10760.
23 Z. Wang, Y. Zhao, J. Chen, M. Chen, X. Li, T. Jiang, F. Liu, X. Yang, Y. Sun and Y. Zhu, *Molecules*, 2023, **28**, 2787.
24 B. K. Oh, E. B. Ko, J. W. Han and C. H. Oh, *Synth. Commun.*, 2015, **45**, 758–766.
25 I. G. Ovchinnikova, G. A. Kim, E. G. Matochkina, M. I. Kodess, N. V. Barykin, O. S. El'tsov, E. V. Nosova, G. L. Rusinov and V. N. Charushin, *Russ. Chem. Bull.*, 2014, **63**, 2467–2477.
26 S. Y. Abbas, K. A. M. El-Bayouki, W. M. Basyouni and E. A. Mostafa, *Med. Chem. Res.*, 2018, **27**, 571–582.
27 I. I. Ponomarev, D. Yu. Razorenov, D. S. Perekalin, P. V. Petrovskii and Z. A. Starikova, *Russ. Chem. Bull.*, 2007, **56**, 154–159.
28 M. A. Khalil, R. Soliman, A. M. Farghaly and A. A. Bekhit, *Arch. Pharm.*, 1994, **327**, 27–30.
29 A. M. Farghaly, R. Soliman, M. A. Khalil, A. A. Bekhit, A. el-Din and A. Bekhit, *Boll. Chim. Farm.*, 2002, **141**, 372–378.
30 C.-L. Sun and Z.-J. Shi, *Chem. Rev.*, 2014, **114**, 9219–9280.
31 K. Morimoto, T. Dohi and Y. Kita, *Synlett*, 2017, 1680–1694.
32 R. Narayan, K. Matcha and A. P. Antonchick, *Chem. – Eur. J.*, 2015, **21**, 14678–14693.
33 W. Wei, Z. Wang, X. Yang, W. Yu and J. Chang, *Adv. Synth. Catal.*, 2017, **359**, 3378–3387.
34 Y. Takeda, R. Kajihara, N. Kobayashi, K. Noguchi and A. Saito, *Org. Lett.*, 2017, **19**, 6744–6747.
35 N. Jatangi, N. Tumula, R. K. Palakodety and M. Nakka, *J. Org. Chem.*, 2018, **83**, 5715–5723.
36 G. Yin, B. Zhou, X. Meng, A. Wu and Y. Pan, *Org. Lett.*, 2006, **8**, 2245–2248.
37 Y.-P. Zhu, M. Lian, F.-C. Jia, M.-C. Liu, J.-J. Yuan, Q.-H. Gao and A.-X. Wu, *Chem. Commun.*, 2012, **48**, 9086.
38 Y. Zhu, F. Jia, M. Liu and A. Wu, *Org. Lett.*, 2012, **14**, 4414–4417.
39 Y. Zhu, Z. Fei, M. Liu, F. Jia and A. Wu, *Org. Lett.*, 2013, **15**, 378–381.
40 Y.-C. Song, W.-H. Cao, M.-X. Wang, R.-Q. Wang, Y.-Y. Sun, A.-X. Wu and Y.-P. Zhu, *J. Org. Chem.*, 2024, **89**, 12832–12841.
41 Y. Song, M. Wang, Y. Yi, Y. Liu, W. Zhang, Z. Wang, Y. Sun, A. Wu and Y. Zhu, *Adv. Synth. Catal.*, 2024, **366**, 1348–1355.
42 D. S. Latha and S. Yaragorla, *Eur. J. Org. Chem.*, 2020, 2155–2179.
43 S. Tang, K. Liu, Y. Long, X. Qi, Y. Lan and A. Lei, *Chem. Commun.*, 2015, **51**, 8769–8772.
44 P. S. Volvoikar and S. G. Tilve, *Org. Lett.*, 2016, **18**, 892–895.
45 P. T. Parvatkar, R. Manetsch and B. K. Banik, *Chem. – Asian J.*, 2019, **14**, 6–30.
46 M. Elagawany, L. Maram and B. Elgendy, *J. Org. Chem.*, 2023, **88**, 17062–17068.
47 M. Elagawany, L. Maram and B. Elgendy, *J. Org. Chem.*, 2024, **89**, DOI: **10.1021/acs.joc.3c01973**.
48 M. Elagawany, L. Hegazy and B. Elgendy, *Tetrahedron Lett.*, 2019, **60**, 2018–2021.
49 M. Elagawany, L. Maram and B. Elgendy, *RSC Adv.*, 2021, **11**, 7564–7569.
50 W. Saaed, M. Elagawany, M. M. Azab, A. S. Amin, N. P. Rath, L. Hegazy and B. Elgendy, *Results Chem.*, 2020, **2**, 100042.

51 B. Draghici, B. E.-D. M. El-Gendy and A. R. Katritzky, *Synthesis*, 2012, 547–550.
52 A. T. Nelson, Y. Wang and E. R. Nelson, *Endocrinology*, 2021, **162**, bqab184.
53 G. Sun, Q. Cui and Y. Shi, in *Current Topics in Developmental Biology*, ed. D. Forrest and S. Tsai, Academic Press, 2017, vol. 125, pp. 257–273.
54 T. Wang and J.-Q. Xiong, *Neurosci. Bull.*, 2016, **32**, 108–114.
55 K. Griffett, G. Bedia-Diaz, L. Hegazy, I. M. S. de Vera, U. S. Wanninayake, C. Billon, T. Koelblen, M. L. Wilhelm and T. P. Burris, *Cell Chem. Biol.*, 2020, **27**, 1272–1284.
56 R. Singhal, S. P. Choudhary, B. Malik and M. Pilania, *RSC Adv.*, 2024, **14**, 5817–5845.
57 K. Griffett, G. Bedia-Diaz, L. Hegazy, I. M. S. de Vera, U. S. Wanninayake, C. Billon, T. Koelblen, M. L. Wilhelm and T. P. Burris, *Cell Chem. Biol.*, 2020, **27**, 1272–1284.
58 P. Kandel, F. Semerci, R. Mishra, W. Choi, A. Bajic, D. Baluya, L. Ma, K. Chen, A. C. Cao, T. Phongmekhin, N. Matinyan, A. Jiménez-Panizo, S. Chamakuri, I. O. Raji, L. Chang, P. Fuentes-Prior, K. R. MacKenzie, C. L. Benn, E. Estébanez-Perpiñá, K. Venken, D. D. Moore, D. W. Young and M. Maletic-Savatic, *Proc. Natl. Acad. Sci. U. S. A.*, 2022, **119**, e2023784119.
59 L. E. Markham, T. Koelblen, H. R. Chobanian, A. V. Follis, T. P. Burris and G. C. Micalizio, *ACS Cent. Sci.*, 2024, **10**, 477–486.
60 X. Zhi, X. E. Zhou, Y. He, K. Searose-Xu, C. L. Zhang, C. C. Tsai, K. Melcher and H. E. Xu, *Genes Dev.*, 2015, **29**, 440–450.
61 X. Corso-Díaz, C. N. de Leeuw, V. Alonso, D. Melchers, B. K. Y. Wong, R. Houtman and E. M. Simpson, *BMC Genomics*, 2016, **17**, 832.
62 Schrödinger LLC, *Schrödinger, LLC*, 2023, preprint, Schrödinger, LLC, 2023–4, **https://www.schrodinger.com/products/maestro**.
63 D. A. Wang, J. Wolf, R. M. Caldwell, J. W. Kollman and P. A. Case, *J. Comput. Chem.*, 2004, **25**, 1157–1173.
64 E. F. Pettersen, T. D. Goddard, C. C. Huang, G. S. Couch, D. M. Greenblatt, E. C. Meng and T. E. Ferrin, *J. Comput. Chem.*, 2004, **25**, 1605–1612.